The chronology of Late Pleistocene thermal contraction cracking derived from sand wedge OSL dating in central and southern France

Eric Andrieux, Mark D Bateman, Pascal Bertran

The chronology of Late Pleistocene thermal contraction cracking derived from sand wedge OSL dating in central and southern France

Eric Andrieux[1], Mark D. Bateman[2], Pascal Bertran[1,3]

[1] PACEA, UMR 5199 Université de Bordeaux – CNRS, Bâtiment B18, Allée Geoffroy-Saint-Hilaire, CS 50023, 33615 Pessac cedex, France. *Email*: andrieux.e@gmail.com

[2] Department of Geography, University of Sheffield, Winter Street, Sheffield S10 2TN, UK. *Email*: m.d.bateman@sheffield.ac.uk

[3] INRAP, 140 avenue du Maréchal Leclerc, 33130 Bègles, France. *Email*: pascal.bertran@inrap.fr

Abstract

Much of France remained unglaciated during the Late Quaternary and was subjected to repeated phases of periglacial activity. Numerous periglacial features have been reported but disentangling the environmental and climatic conditions they formed under, the timing and extent of permafrost and the role of seasonal frost has remained elusive. The primary sandy infillings of relict sand-wedges and composite-wedge pseudomorphs record periglacial activity. As they contain well-bleached quartz-rich aeolian material they are suitable for optically stimulated luminescence dating (OSL). This study aims to reconstruct when wedge activity took place in two regions of France; Northern Aquitaine and in the Loire valley. Results from single-grain OSL measurements identify multiple phases of activity within sand wedges which suggest that wedge activity in France occurred at least 11 times over the last 100 ka. The most widespread events of thermal contraction cracking occurred between ca. 30 and 24 ka (Last Permafrost Maximum) which are concomitant with periods of high sand availability (MIS 2). Although most phases of sand-wedge growth correlate well with known Pleistocene cold periods, the identification of wedge activity during late MIS 5 and the Younger Dryas strongly suggests that these features do not only indicate permafrost but also deep seasonal ground freezing in the context of low winter insolation. These data also suggest that the overall young ages yielded by North-European sand-wedges likely result from poor record of periglacial periods concomitant with low sand availability and/or age averaging inherent with standard luminescence methods.

Keywords: OSL; Luminescence dating; Sand wedge; Thermal contraction cracking; France

1. Introduction

Globally during the last glacial periglaciation extended from high to mid-latitude areas driven by overall climatic coolings. Areas beyond the ice limits experienced multiple periglacial phases and have records of these events preserved in the surficial sediments and landforms (Isarin et al., 1998; Andrieux et al., 2016a). A long-standing challenge has been to establish the relationship between preserved structures and periglacial processes and climate (e.g. Williams, 1968; Péwé, 1966; Vandenberghe, 1983; Kasse and Vandenberghe, 1998; Murton et al., 2000; Murton, 2013). This has led to attempt to model the style and extent of periglaciation in mid latitudes (e.g. Tricart, 1956; Maarleveld, 1976; Huijzer and Vandenberghe, 1998; Van Vliet-Lanoë and Hallégouët, 2001; Vandenberghe et al., 2004; 2014). A second challenge has been to understand the timing and extent of these relict periglacial features to enable linkages with other palaeoclimatic proxy records and to better understand spatial regional differences. Previous works (e.g. Buylaert et al., 2009) have undertaken this at the region scale but such studies are hampered by the often polycyclic nature of periglacial features.

The age of when ice and sand wedges formed remains uncertain so far in France and available data are often marred by large uncertainties. The secondary nature of the infilling of ice wedge pseudomorphs does not allow direct dating, and age estimates generally rely on bracketing dates obtained from host and cover sediments. Primary infillings in sand wedges are composed of quartz-rich aeolian material, which is suitable for optically stimulated luminescence (OSL) dating. Sand wedges are, however, far from being readily datable features. Standard OSL methods applied to a sample of sandy infilling, i.e. a cylinder 5 cm in diameter and 20 cm long, make sense only if all the sand grains have a similar depositional history. Studies in modern arctic settings suggest that such an assumption is probably not true in most cases. As shown by Mackay (1993), thermal contraction cracking occurs episodically. The millimetre-thick vertical sand laminae may thus reflect successive, discrete episodes of cracking and filling, which are potentially separated by long phases of wedge inactivity.

Accordingly, recent studies by Bateman (2008) and Bateman et al. (2010) pointed that OSL dating of sand wedges shows sometimes palaeodose (De) scatter that cannot be explained by other experimental parameters such as poor recycling, sensitivity changes, variable OSL components, recuperation problems, or large De uncertainties from dim grains. This scatter may be related to

multiple De components as it would be the case in a multi-phase formation model for the wedges. Consequently, the ages calculated from luminescence values yielded by aliquot measurement or/and Central Age Model analysis (CAM, Galbraith et al., 1999) may not necessarily represent the true ages of the features but rather averaged values. The use of high resolution single grain measurements and the extraction of the datasets with Finite Mixture Model (FMM, Galbraith and Green, 1990), which was developed to analyse statistically data comprising multiple components, allow for the calculation of more representative ages (Bateman et al., 2010, 2014; Guhl et al., 2013).

This present study aims to establish for the first time a chronological framework for periglacial wedge formation in France during the Late Pleistocene. Following the approach proposed by Bateman et al. (2010), single grain OSL measurements and FMM analysis were applied to a comprehensive suite of 33 samples taken from the infillings of French sand-wedges and composite-wedge pseudomorphs in order to better understand the chronology of Late Pleistocene thermal contraction cracking events. The features selected are from a number of sites located within two regions, one in Northern Aquitaine which is one of the southernmost areas of sand-wedge occurrence in France (~45°N), the other in the Loire valley in a more northern region (~47°N) (Figure 1).

2. Background

Relict periglacial wedge structures and pseudomorphs created by thermal contraction cracking in areas that underwent permafrost and/or deep seasonal freezing of the ground have been widely reported in France (Fig. 1). Ice-wedge pseudomorphs characterised by a secondary infilling replacing ice have been described in alluvial deposits of the Paris basin and in loess of northern France (e.g. Michel, 1969, 1975; Sommé and Tuffreau, 1971; Lautridou, 1985; Antoine, 1988, 1990; Lécolle, 1989; Deschodt et al., 1998; Sellier and Coutard, 2007; Feray, 2009; Moine et al., 2011; Andrieux et al., 2016a,b). These features are only found north of 47.5°N, and demonstrate that part of the territory was affected by permafrost during the coldest periods of the Pleistocene (Andrieux et al., 2016a). Relict epigenetic sand wedges have been discovered between 47.5 and 43.5°N in the vicinity of coversands in the Loire valley, Northern Aquitaine and Provence (Bouteyre and Allemann, 1964; Arnal, 1971; Antoine et al., 2005; Lenoble et al., 2012; Bertran et al., 2014; Andrieux et al., 2016a,b). Unlike ice-wedge pseudomorphs, they show a laminated or massive primary infilling of aeolian sand. Composite wedge pseudomorphs that have both primary and secondary infilling have also been described (Antoine et al., 2005; Andrieux et al., 2016a,b) but difficulties in identifying secondary infillings in sandy sedimentary contexts may have lead to the classification of a large number of these features as ‘sand wedges’ (Andrieux et al., 2016b).

In Europe, North America and Asia, thermoluminescence (TL), infrared-stimulated luminescence (IRSL) and optically-stimulated luminescence (OSL) have been already applied for dating sand wedges on K-feldspars, polymineral fine grains or quartz, using multiple aliquots or single aliquots approaches. Although different techniques were used that does not ensure data homogeneity, the calculated ages provide a first chronological framework for sand wedge development during the Late Pleistocene. The largest set of OSL ages has been obtained by Buylaert et al. (2009) from 14 sand and composite-wedge pseudomorphs in Flanders, Belgium. The results suggest that most wedges (i.e. 12 out of 14) were active between 21.8 ± 1.2 and 13.9 ± 1.0 ka. This is in agreement with the previously published ages for northern Europe (Böse, 1992, 2000; Briant et al., 2005; Kjaer et al., 2006; Kasse et al., 2007), which show that the features mostly formed during MIS 2 and the Lateglacial. Few ages fall within MIS 3 (Kolstrup and Mejdhal, 1986; Kolstrup, 2007; Christiansen, 1998). More to the south (47.64°N), two sand wedges also yielded late MIS 2 ages in Hungary (Kovàcs et al., 2007; Fàbiàn et al., 2014). The published OSL ages for French sand wedges (ca. 45°N) are on average older and cluster between 37 and 23 ka (Guhl et al., 2013; Lenoble et al., 2012; Bertran et al., 2014). Although being part of the same polygonal network visible in aerial photographs, all the investigated wedges yielded different ages which cannot be explained by luminescence dating uncertainties. This strongly suggested that sand wedge growth was asynchronous and controlled by local conditions rather than global.

A number of cross-sections in loess from northern France, Belgium and Germany show networks of ice-wedge pseudomorphs which open generally in iron-depleted and cryoturbated horizons referred to as “tundra gleys” (i.e. Haplic Cryosols according to Kadereit et al., 2013). These serve as benchmark levels for the correlation between sections at a regional scale in northern France (Antoine and Locht, 2015). The few reliable numerical ages in direct association with the pseudomorphs highlight six events of permafrost development. The main phase is characterized by two levels of large ice wedge pseudomorphs, sometimes superimposed, and dated to ca. 25 and 30 ka respectively (Frechen et al., 2001; Locht et al., 2006; Kreutzer et al., 2012; Meszner et al., 2013; Antoine et al., 2015). This period stretches over Greenland Stadials (GS) 3, 4 and 5 (Rasmussen et al., 2014)and can be interpreted as the Last Permafrost Maximum (LPM, Vandenberghe et al., 2014). Three other levels of ice-wedge pseudomorphs associated with tundra gleys have been identified in France at Havrincourt (northern France, Antoine et al., 2014): (1) small pseudomorphs at the top of the sequence, which remain undated but are stratigraphically younger than the LPM, (2) pseudomorphs in between two soil complexes dated respectively to 42.1 ± 2.8 and 51.5 ± 3.2 ka, and (3) small pseudomorphs bracketed between 61.7 ± 4 and 65 ± 3.8 ka.

These ages depict a complex formation history and differ from those published for sand wedges in Northern Europe, which are unexpectedly much younger.

3. Study sites

The precise location of the studied features, the sample name and the lab codes are given in table 1. The sites of Salaunes (Château Montgaillard), Cussac-Fort-Médoc (Parcelle Lagrange), Mérignac (Chronopost) and Saint-André-de-Cubzac (ZAC Parc d'Aquitaine) are situated on the plateaus surrounding the Garonne valley (Salaunes, Saint-André-de-Cubzac) or on old alluvial terraces (Cussac-Fort-Médoc, Mérignac). The Eocene to Lower Pleistocene host sediment ranges from clayey sand to sandy gravel. All the studied wedges are epigenetic features filled with aeolian sand near the margin of Pleistocene coversands. The wedges open at the top of alluvial deposits usually capped by ventifacts. They are V-shaped, 1 to 2 m in depth, 0.3 to 0.6 m in width (measured orthogonally to the axial plane of the wedge), and have either a massive or a laminated sandy infilling (Figure 2). In total, 17 samples were gathered from 5 sand wedges in these sites.

In the Loire valley 16 samples were taken from 6 epigenetic sand wedges (Olivet, La Flèche, La-Chapelle-aux-Choux, Challans) and 2 composite wedge pseudomorphs (Durtal, Sainte-Geneviève-des-Bois) (table 1, Figure 2). The wedges developed within Pleistocene alluvial terraces composed of sandy gravel, in close proximity of rivers which provided abundant aeolian sand during the glacials. The wedges are 0.3 to 1 m wide and 1 to 2.5 m in depth. At Durtal a primary laminated sandy infill (0.3 m wide, 1.7 m depth) cross-cuts a previous secondary infill composed of massive sandy gravel (1 m wide, 2 m in depth). The composite-wedge pseudomorph at Sainte-Geneviève-des-Bois, 1.2 m wide and 1.7 m in depth, shows a primary massive sandy infill cross-cut by a secondary silty infill which exhibits U-shaped lamination. The site of Saint-Christophe-du-Ligneron (Challans) is located south of the Loire estuary in the vicinity of a small coversand area.

4. Methodology

4.1 Sample collection and preparation

Thirty-three samples were collected for OSL from the sandy infillings of freshly exposed sand wedges or composite wedge pseudomorphs by hammering in the sections opaque PVC tubes or metal tubes (60 mm in diameter, 250 mm long). To get a better chance of recording different events potentially preserved in the wedges multiple samples were taken along a horizontal line in the infilling of each

wedge when possible. Vertical samples were taken within the primary infillings to check for the influence of depth on doses. The host sediments were also sampled for gamma dose rate modelling purposes.

The samples were prepared under subdued red light conditions at the Sheffield Luminescence Laboratory. To avoid any potential light contamination that may have occurred during sampling, 2 cm of sediment located at the ends of the PVC tubes was removed and used for estimations of palaeomoistures. The light-unexposed material was treated with hydrochloric acid (1m, HCl) and hydrogen peroxide (H_2O_2) to remove carbonates and organic matter. To ensure that only one grain will fit into each hole when mounted on discs for single grain analysis and to minimise intra-sample variability dry sieving of the sediment was performed, and the 180-250 µm fraction size was kept for OSL measurement. Heavy liquid treatment with sodium polytungstate at 2.67 $g.cm^{-3}$ allowed the separation of quartz from sediment of higher specific gravity (i.e heavy minerals). The remaining sediment was then treated with hydrofluoric acid (HF) to etch the grain surface and to remove residual feldspars and light minerals other than quartz. Once dry, the sediment was treated again with HCl, and then re-sieved at 180 µm to remove acid-soluble fluorides and any grains that have been significantly reduced in size by etching.

4.2 Dose rate determination

Dose rates to individual samples are based on elemental measurements made using inductively-coupled plasma mass spectrometry (ICP-MS) as in situ gamma-spectrometer were not possible. This was carried out at the laboratories of SGS Canada (www.sgs.ca). Insofar as most wedges are less than 0.5 m in width, it was generally not possible to sample 0.3 m away from the host sediment, which is the maximum travelled distance by gamma rays. Therefore, the adjacent different lithostratigraphic units of host sediment were also measured to establish their contribution to the gamma dose rate. Gamma dose rates were modelled and corrected using the scaling factors of Aitken (1985) and had little impact on the total doses. Elemental concentrations were converted to annual dose rates using data from Guérin et al. (2011). In order to adjust the dose rates, the following attenuation factors were used: (i) alpha and beta grain size attenuation effects from Bell (1980), Mejdhal (1979) and Readhead (2002), (ii) an a-value of 0.10 ± 0.02 for coarse grain quartz (Olley et al. 1998), (iii) an etch attenuation factor after Duller (1992), and (iv) an attenuation for palaeomoisture content based on moisture content at time of sampling with an absolute error of ± 5% incorporated to allow for past changes. The contribution to dose rates from cosmic sources is a function of geographic location, burial depth and altitude and was calculated using the algorithms published in Prescott and Hutton

(1994). An internal quartz dose rate of 10 µGy/ka was added to the total dose rate as done by Vandenberghe et al. (2008).

Beta heterogeneity may occur due to spatial variability in the concentration of beta emitters coupled with the short penetration range of beta particles (ca. 3mm, Aitken, 1998). For example feldspars grains with high ^{40}K concentrations can be scattered at low abundance within quartz dominated sediment and result to beta doses variations at the grain scale. This is the subject of ongoing research and modelling (Martin et al., 2015a, b). In the present study, this type of beta heterogeneity was considered as a minor contributory factor only since the samples were collected from homogeneous well mixed aeolian sand.

The dosimetry results are available in table 2.

4.3 Luminescence measurements

Luminescence measurements were performed on a Risø reader TL-DA-15 equipped with a 90Sr/90Y beta source for irradiation (Bøtter-Jensen et al., 2003). The reader was fitted with a single grain attachment that used a 10 mW Nd:YVO4 solid state diode-pumped laser emitting at 532 nm, which produced a spot approximately 50 µm in diameter (Duller et al., 1999), allowing simulation of individual grains. The luminescence emissions were detected through a Hoya U-340 filter. The purity of extracted quartz was tested for each sample by stimulation with infra-red light as per Duller (2003). No samples showed signs of feldspar contamination. Single grains were measured on 9.6 mm diameter aluminium discs containing 100 holes.

Equivalent dose (D_e) determination was carried out using the Single-Aliquot Regenerative-dose (SAR; Murray and Wintle, 2000, 2003; Table A1). A four point SAR protocol was employed to bracket the expected palaeodoses with an additional recycling point to check for uncorrected sensitivity changes (Figure A1). Preheat temperatures were determined using a dose recovery preheat plateau test (Murray and Wintle, 2003). The samples displayed OSL decay curves dominated by the fast (bleachable) component, had good dose recovery, low thermal transfer and good recycling (Figure A2). D_e values were only accepted when the recycling ratio was comprised between 0.8 and 1.2, recuperation on zero dose was lower than 5%, and the error on the D_e was less than 30%. The grains exhibiting a signal that was not possible to fit by an exponential, or exponential plus linear growth

curve were rejected. However, when the palaeodose could not be ascertained for a grain due to saturation it was recorded as it gives important information on the sample. A minimum of 50 D_e values which met the quality acceptance criteria were measured for each sample to ensure a representative spread in D_e values and to assess the degree of scatter and skewness of the data. Only 2 to 4% of the grains had a measurable OSL signal that met the selection criteria. The samples CAH2.1, CAH2.2, CAH2.3, CAH4.1 and CAH4.2 from the Loire valley had between 10 to 20% saturated grains, whereas the samples from Northern Aquitaine do not show any saturation. Potential contamination by host material was checked during sampling and preparation. No evidence for mixing of different material was found.

The measurements of the OSL signal at single grain level show a large D_e heterogeneity with high overdispersion (Figure 3; Figure A3). As for the sand wedge investigated by Bateman et al. (2008, 2010) the scatter of the D_e values cannot be explained by poor recycling, recuperation problems, or sensitivity changes. In few sampled wedges sand lamination was visible, which testifies to the lack of post-depositional perturbation of the primary infilling. However, a significant amount of the samples were taken from massive sand bodies or from infillings where lamination was only locally preserved, which probably indicate that subsequent mixing occurred due to ice thaw, bioturbation and other pedoturbations (Murton et al., 2000). Such processes may have lead to the inclusion of partially bleached grains in the wedges coming from the surrounding ground surface or from the host sediment, which can result in long tails of D_e or in broad distributions rather than in discrete peaks. The scatter of data is thus assumed to be caused either by poor bleaching of grains prior burial or by the mixing of different age deposits.

An averaging issue would arise if the Central Age model (CAM; Galbraith et al., 1999, Roberts et al., 2000) was used to extract the D_e values since this model is designed for well-bleached samples. The standard approaches are to use either the Minimum Age Model (MAM; Galbraith and Laslett, 1993) or the Finite Mixture Model (FMM; Galbraith and Green 1990) to calculate age estimates. FMM allows the extraction of De components within De distributions and MAM extract the component that provide the minimum age. In our case this means that FMM date the different periods of periglacial wedge infilling while MAM gives the estimate of the last time the wedge was active. Both models were used to calculate the age estimates of the wedges. However, FMM was considered more appropriate because of the potential multi-phased nature of sand-wedges. As the CAM is the model used in previous dating of sand-wedges, the CAM ages were calculated for comparison purposes.

Dose recovery tests performed on multiple samples coming from different wedges (Figure A4) showed less than 10% of data scatter for a given dose. Therefore, for FMM a σ_b value of 0.15 was chosen. The best fit was assessed by iteratively increasing the number (k) of components until the closest to zero value of the Bayesian Information Criterion (BIC) was reached. To avoid the influence of potential post-contamination the D_e components were considered only when exceeding 10% of the total D_e values for each sample (Bateman et al., 2007).

5. Results

FMM analysis allowed extraction of two to four components for each of the 33 samples from which a total of 86 age estimates were calculated, 47 in the Loire valley and 39 in Northern Aquitaine respectively (table 3). The OSL ages range between 337 ± 40 ka and 7.5 ± 1.2 ka.

In order to test the assumption that wedge activity was not random during the last glacial but rather occurred during specific, climate-controlled periods, the cumulated probability density of the ages was calculated using Oxcal 4.2 (Bronk Ramsey, 2013) with the expectation that peaks would emerge from the probability distribution. As this was the case, the distribution was adjusted to a combination of Gaussian functions using the software Fityk 0.9.8 (Wojdyr, 2010) and their respective contribution was calculated. The goodness of fit was assessed using R^2, which reached almost unity (R^2=0.9999). The standard deviation of the distribution around the centre of each Gaussian function was estimated from the Full Width at Half Maximum (FWHM). The Probability Density Function (PDF) was plotted together with the NGRIP δO^{18} data over the last 100 ka tuned to the revised Greenland Ice Core Chronology proposed by Rasmussen et al. (2014) to compare the thermal contraction cracking events with known cooling occurrences over Europe (Figure 4).The results suggest the following:

i) The sand wedges and composite wedge pseudomorphs were repeatedly active during the Middle and Late Pleistocene up to the beginning of the Holocene.
ii) The oldest events are recorded in the Loire valley where 71% of OSL ages fall within MIS 3, 4 and 5. In contrast, MIS 2 represent up to 54% of the total OSL ages in Northern Aquitaine. In the latter area, the oldest age falls within MIS 4.
iii) A total of 11 peaks of wedge activity have been extracted from the 86 ages provided by the samples from the whole dataset during the last 100 ka, i.e. 8.5 ± 0.6, 11.9 ± 0.5, 15.3 ± 0.4, 17.4 ± 0.7, 20.7 ± 0.7, 24 ± 1.1, 30 ± 2.5, 42.5 ± 1.9, 56.2 ± 4, 71.4 ± 1.8, 86 ± 4.2 ka

iv) Seven OSL ages are older than 100 ka and may correspond to cracking events that occurred during MIS 6, 8 or 10.

The PDFs of the estimates calculated with the different age models (i.e. CAM, MAM, and FMM) allow for comparisons (Figure 5).Differences between the models are evident. As expected the CAM based dataset by averaging all grains from samples identifies fewer more prominent phases of wedge activity during MIS 2. The MAM based dataset by selecting only the youngest component of grains from a sample, under-estimates the earlier phases of wedging. The FMM datasets by attempting to isolate similar age components within samples provides a longer record with more phases within it.

As shown on a representative case study in figure 6, the calculated ages are much younger than the host material of the wedges. They overlap from one sample to another within the same wedge, and between different wedges, and they are not dependent on depth.

6. Discussion

6.1. France

The overall age distribution of periglacial wedges shows repetitive thermal contraction cracking over the last 100 ka. However, substantial differences emerge from the comparison between the two regions. Two main factors may be involved, which include:

(1) The latitude of the investigated wedges. As expected, the Loire valley yields a larger number of ages falling into MIS 5 to 3 than does Northern Aquitaine which is located at lower latitude. Overall, the first area is assumed to have been more frequently affected by deep seasonal freezing and/or permafrost during the Late Pleistocene.

(2) The sand availability. In addition to the temperature drop that triggers thermal contraction cracking, the main limiting factor in the growth of sand-wedges is the sand supply. In the Loire valley the sand has a fluvial origin, and sand drifting was probably active during the stadials all along the last glacial on bare alluvial deposits exposed to deflation. In contrast, the location of the sand wedges of Northern Aquitaine near the margin of the coversands (“Sables des Landes” Formation, Sitzia et al., 2015) strongly suggests that this formation, which was fed by deflation on the continental plateau exposed during sea-level lowstands, was the main sand source that filled the contraction cracks. Available chronological data (Bertran et al., 2011; Sitzia et al., 2015) show that the coversands built up mostly between ca. 24 and 14 ka. Comparison between the distribution of ages for coversands and sand wedges points to strong similarity, suggesting that the latter primarily

record periods where thermal contraction cracking and voluminous sand drifting in the coversand area occurred at once (Figure 7). To a certain extent, this record may, therefore, be biased toward MIS 2 which corresponds to the main phase of coversand emplacement.

Age clusters were identified in both areas within the Lateglacial (12 ka, i.e. Younger Dryas, 5 dates in whole data set) and, more surprisingly, within the early Holocene at 8.5 ka (5 dates). Since the De components of the early Holocene are only slightly above the 10% chosen threshold, it cannot be excluded that these ages reflect sample contamination due to localised bioturbation. Wedge activity during the Younger Dryas, which were typified by mean annual air temperatures too high for permafrost development in France (Renssen and Isarin, 1998; Simonis et al., 2012), reinforces the assumption that these features are poor indicators of past permafrost as already suggested by Andrieux et al. (2016a) and Wolfe et al. (2016). Younger Dryas mean January air temperature are poorly constrained by available biological records, however, beetle proxies (Ponel et al., 2007) point to rather cold winters (min January temperatures estimated between -3 to -18°C), probably because of low winter insolation (Berger, 1978). This allowed deep seasonal ground freezing to occur. Sand drifting was still active in European coversand areas during the Younger Dryas (Kasse, 2002; Sitzia et al., 2015). In Aquitaine, fields of parabolic dunes developed on large areas at that time (Bertran et al., 2011). More recent sand wedge activity was unexpected, since temperatures rose significantly in the early Holocene, although the seasonal contrast remained high compared to present. Considering the uncertainty associated with the OSL ages and assuming that these ages do not reflect contamination, we suggest here that the recorded thermal contraction events reflect the impact of the short cooling events identified at 9.3 and 8.2 ka in the Greenland ice cores (Rasmussen et al., 2014) and in other proxy records (Wanner et al., 2011). They would also indicate that sand was still mobile at least locally and not yet totally fixed by vegetation.

MIS 2 is a period characterized by strong wedge activity, and includes up to 54% of the ages (i.e. 21 dates) of the Northern Aquitaine data set (phases 3 to 6, Fig. 4). Both regions record wedge formation at the beginning and in the middle of Greenland Stadial 2 (GS 2.1) around respectively 17.5 ka (GS 2.1a) and 21 ka (GS 2.1c), and around 24 ka at the end of GS 3. Another cluster is identified at 15.5 ka (late GS 2.1) only in Northern Aquitaine. The absence of record of this contraction cracking phase in the Loire valley may be explained as follows:

(1) Sand availability and/or deflation were limited in regions distant from the main coversand areas. However, the reason why this occurred specifically during this period remains hard to explain.
(2) The higher number of ages obtained in Northern Aquitaine allows better precision in the calculation of peaks, which are typified by low FWHM. This highlights the sensitivity of the method

used for identifying the major phases of wedge growth to the size of the data set. Further dating will make it possible to improve the representativeness of the identified phases.

A period of widespread thermal contraction cracking which is common to both study areas is also recorded during the end of MIS 3 at approximately 30 ka (GS 5) (phase 7, Fig. 4). Older wedge activity is mostly detected in the Loire valley. Clustering of ages appears less obvious, however, and the identified phases have to be considered with caution. The most preeminent phase took place at ~56 ka, i.e. probably at the very end of MIS 4 taking into account the luminescence dating uncertainties (phase 9, Fig. 4). It is worth noting that a significant number of ages (6 dates) fall within late MIS 5 which was typified on average by a mild climate. PDF analysis suggests that they cluster around ~86 ka, i.e. during the stadial GS 22 (phase 11, Fig. 4) . As for the early Holocene, this period coincides with a minimum in winter insolation (Berger, 1978).

Although it is not possible to define D_e values for saturated grains, their presence within the investigated wedges is interpreted as reflecting phases of thermal contraction cracking that are beyond the limit of the luminescence dating method on quartz. The saturated grains come from samples that provided the oldest ages, i.e. MIS 8 or 10.

In some wedges (Salaunes, Mérignac and Cussac-Fort-Médoc) the samples taken from the sides of the infilling have yielded older ages than those from the middle. This has to be interpreted as the preferred preservation of early phases of activity in the sides of the wedges.

6.2. Comparison with the records of Northern Europe

The analysis presented here show that the thermal contraction events previously identified in the loess deposits of northern France were also recorded in the sand wedges and composite wedge pseudomorphs from southwest France and the Loire valley. Particularly, the two main levels of large ice-wedge pseudomorphs dated to 30 and 25 ka (Antoine et al., 2014; Bertran et al., 2014) in the loess sequences have their counterparts in sand wedges (ca. 30 and 24 ka respectively). Such a synchronicity testifies to widespread events of thermal contraction cracking in France, which are thought to coincide with the last maximum of permafrost extension. In the marine realm, these events correspond to Heinrich Stadials 3 and 2 respectively (Sanchez-Goñi and Harrison, 2010). Because of the scarcity of available ages, more in detail fitting of the records remains impossible both for older and younger phases. Overall, the number of the phases of wedge development appears to be larger in the sand wedges than in loess. The following factors may be involved:

(1) Poor preservation of ice-wedge pseudomorphs due to thermokarst processes (Locht et al., 2006). Strong pedoturbation at the top of loess sequences during the Holocene may also have obscured or made illegible MIS 2 features.

(2) Lack of permafrost and associated growth of large ice bodies susceptible to produce pseudomorphs. Thermal contraction cracking in the context of deep seasonal freezing of the ground created sand wedges where sand drifting was active, but only tiny fissures elsewhere. This was especially the case for Late MIS 5 and the Lateglacial.

Using a same approach to that used here on periglacial patterned ground (polygons and stripes) found in East Anglia, UK, Bateman et al. (2014) found similar phases of activity during the last 90 ka at 55–60 ka (MIS 4), 31–35 ka (MIS 3), 20–22 ka (GS2.1c) and 11–12 ka (GS1). However, most of the previous age estimates for sand wedges from northern Europe fall within late MIS 2 and the Lateglacial, i.e. during the main periods of coversand emplacement. In contrast to loess sequences, almost no wedge activity is recorded within late MIS 3 and early MIS 2. In the light of our data, this pattern has to be interpreted as reflecting two main factors: (1) limited record of thermal contraction phases during periods with low sand availability, (2) the use of aliquot and/or CAM analysis for the calculation of age estimates, which led to averaging the signal. This skewed the ages in favour of the most prominent phases of activity and hampered identification of the multiple events of sand wedge growth. Although a few studies in North America have suggested that distinct generations of sand wedges or multi-phased wedges occurred (French et al., 2003; Bateman et al., 2010), multiple-dose populations within wedges in Europe (Kolstrup, 2004) or unexpected ages were often attributed to partial bleaching of the sand grains due to sediment mixing and were thus rejected.

7. Conclusion

The application of single grain OSL to 33 samples taken from sand and composite wedges in France allowed identifying of multi-phased thermal contraction events within single preserved wedge features. FMM analysis identified two to four components for each sample and resulted in the calculation of 86 age estimates, each corresponding to a period of ground cracking. These show that wedges were active during Late Pleistocene cooling periods when thermal contraction and sand drifting in the coversand areas occurred at the same time, i.e. dominantly during MIS 2. Synchronicity between the ages provided by ice-wedge pseudomorphs, sand-wedges and composite-wedges in France testifies to widespread events of thermal contraction cracking between ca. 30 and 24 ka (Last Permafrost Maximum). Late MIS 5 and Younger Dryas events also suggest that wedging occurred in connection with deep seasonal ground freezing during phases with marked seasonality. In

comparison, the mainly late MIS2 – Younger Dryas ages of North-European sand wedges are thought to reflect poor recording of the periods with low sand supply. In addition, the potential averaging issue inherent with the use of aliquots and CAM analysis for the dating of sand-wedges may have biased the ages towards the major phases of activity and have hampered the identification of multiple periods of opening.

By providing the first chronological framework for thermal contraction cracking in France, this study shows that sand-wedges and composite-wedge pseudomorphs are significant, but complex archives of the Pleistocene periglacial environments. Our results allow reassessing the periglaciation of France and its timing across Western Europe. However, owing to OSL uncertainties more effort in dating is required to improve the accuracy of the identified phases of thermal contraction cracking. The multiplication of study areas in Europe should also make it possible to highlight the latitudinal fluctuations of periglacial processes during the last glacial.

Aknowledgements

This work benefitted from funds provided by the Institut National de Recherches Archéologiques Préventives (Inrap), the Lascarbx (program of the Agence National de la Recherche ANR-10-LABX-52), the University of Bordeaux, and the PACEA laboratory. EA wishes to acknowledge the department of Geography, University of Sheffield, whilst a visiting scientist. Robert Ashurst and Alicia Medialdea are also thanked for their assistance in preparing and dating the samples.

References

Aitken, M.J., 1985. Thermoluminescence dating. Academic Press, Orlando, Florida, 359 p.

Aitken, M.J., 1998. An introduction to Optical Dating. The dating of Quaternary Sediments by the Use of Photo-Stimulated Luminescence. Oxford University press, Oxford. 267 p.

Andrieux, E., Bertran, P., Saito K., 2016a. Spatial analysis of the French Pleistocene permafrost by a GIS database. Permafrost and Periglacial Processes, 27 (1), 17-30.

Andrieux, E., Bertran, P., Antoine, P., Deschodt, L., Lenoble, A., Coutard, S., 2016b. Database of pleistocene periglacial features in France: description of the online version », Quaternaire, 27/4, 329-339.

Antoine, P., 1988. Contribution à l'étude des loess du Pléistocène supérieur du bassin de la Somme. Revue Archéologique de Picardie 1-2, 25-44.

Antoine, P., 1990. Chronostratigraphie et environnement du Paléolithique du Bassin de la Somme. Publication du centre d'Etude et de Recherches Préhistoriques de Lille (CERP) 2, 231 pp.

Antoine, P., Marchiol, A., Brocantel, M., Gros Y., 2005. Découverte de structures périglaciaires (sand-wedges et composite-wedges) sur le site de stockage de déchets radioactifs de l'Aube (France). Comptes Rendus Géosciences, 337 (16), 1462-1473.

Antoine, P., Goval, E., Jamet, G., Coutard, S., Moine, O., Hérisson, D., Auguste, P., Guérin, G., Lagroix, F., Schmidt, E., Robert, V., Debenham, N., Meszner, S., Bahain, J.J., 2014. Les séquences Loessiques Pléistocène supérieur d'Havrincourt (Pas-de-Calais, France) : stratigraphie, paléoenvironnements, géochronologie et occupations paléolithiques. Quaternaire, 4, p. 321-368.

Antoine, P., Locht, J.L., 2015. Chronostratigraphie, paléoenvironnements et peuplements au Paléolithique moyen : les données du nord de la France. Mémoire de la Société Préhistorique Française , 59 , 11-23.

Antoine, P., Moncel, M.H., Locht, J.L., Limondin-Lozouet, N., Auguste, P., Stoetzel, E., Dabkowski, J., Voinchet, P., Bahain, J.J., Falgueres, C., 2015. Dating the earliest human occupation of Western Europe: New evidence from the fluvial terrace system of the Somme basin (Northern France). Quaternary International, 370, 77-99.

Arnal, H., 1971. Les sols polygonaux étirés et sols striés d'âge würmien de Laudun (Gard). Bulletin de l'Association Française pour l'Etude du Quaternaire, 8 (3), 151-160.

Bailey, R.M., Arnold, L.J., 2006. Statistical modelling of single grain quartz De distributions and an assessment of procedures for estimating burial dose. Quaternary Science Reviews, 25, 2475-2502.

Bateman, M.D., 2008. Luminescence dating of periglacial sediments and structures: a review. Boreas 37, 574-588.

Bateman, M.D., Boulter, C.H., Carr, A.S., Frederick, C.D., Peter, D., Wilder, M., 2007. Preserving the palaeoenvironmental record in Drylands: Bioturbation and its significance for luminescence derived chronologies. Sediment Geology, 195, 5-19.

Bateman, M.D., Hitchens, S., Murton, J.B., Lee, J.R., Gibbard, P.L., 2014. The evolution of periglacial patterned ground in East Anglia, UK. Journal of Quaternary Science, 29, 301–317.

Bateman, M.D., Murton, J.B., Boulter, C., 2010. The source of De variability in periglacial sand wedges: Depositional processes versus measurement issues. Quaternary Geochronology, 5, 250-256.

Bell, W.T., 1980. Alpha attenuation in Quartz grains for Thermoluminescence Dating. Anc. TL 12, 4-8.

Berger, A., 1978. Long-term variations of daily insolation and Quaternary climatic changes. J. Atmos. Sci., 35(12), 2362–2367.

Bertran, P., Bateman, M., Hernandez, M., Lenoir, M., Mercier, N., Millet, D., Tastet, J.P., 2011. Inland Aeolian deposits of southwest France: facies, stratigraphy and chronology, Journal of Quaternary Science, 26, 374-388.

Bertran, P., Andrieux, E., Antoine, P., Coutard, S., Deschodt, L., Gardère, P., Hernandez, M., Legentil, C., Lenoble, A., Liard, M., Mercier, N., Moine, O., Sitzia, L., Van Vliet-Lanoë, B., 2014. Distribution and chronology of Pleistocene permafrost features in France: database and first results. Boreas, 43 (3), 699-711.

Böse, M., 1992: Late Pleistocene sand-wedge formation in the hinterland of the Brandenburg stade. Sveriges Geologiska Undersökning Series Ca 81, 59-63.

Böse, M., 2000. Gravel analysis of Weichselian tills and OSL dates of sand wedges in western Poland. Quaestiones Geographicae 21, 39-44.

Bøtter-Jensen, L., Andersen, C.E., Duller, G.A.T., Murray, A.S., 2003. Developments in radiation, stimulation and observation facilities in luminescence measurements. Radiation Measurement 37, 535-541.

Bouteyre G., Allemann M., 1964. Sur quelques phénomènes périglaciaires en Costières du Gard. Un réseau polygonal de fentes en coin. Bulletin de la Société des Sciences Naturelles de Nimes L, 84-96.

Briant, R.M., Bateman, M.D., Russell Coope, G., Gibbard, P.L., 2005. Climatic control on Quaternary fluvial sedimentology of a Fenland Basin river, England. Sedimentology, 52, 1397-1423.

Bronk Ramsey, C., Lee, S., 2013. Recent and Planned Developments of the Program OxCal. Radiocarbon, 55(2-3), 720-730.

Buylaert, J.P., Ghysels, G., Murray, A.S., Thomsen, K.J., Vandenberghe, D., De Corte, F., Heyse, I., Van den Haute, P., 2009. Opticla dating of relict sand wedges and composite-wedge pseudomorphs in Flandders, Belgium. Boreas, 38, 160-175.

Christiansen, H.H., 1998. Periglacial sediments in an Eemian–Weichselian succession at Emmerlev Klev, southwestern Jutland, Denmark. Palaeogeography, Palaeoclimatology, Palaeoecology 138, 245–258.

Deschodt, L., Djemmali, N., Drwila, G., Feray, P., Teheux, E., 1998. Onnaing (59), usine Toyota. 62 pp. Rapport des sondages archéologiques profonds, Inrap, Amiens.

Duller, G.A.T., 1992. Luminescence Chronology of Raised Marine Terraces, South-West North Island, New Zealand. PhD thesis. University of Wales, Aberystwyth.

Duller, G.A.T., 2003. Distinguishing quartz and feldspar in single grain luminescence measurements. Radiation Measurements 37, 161-165.

Duller, G.A.T., Bøtter-Jensen, L., Murray, A.S., Truscott, A.J., 1999. Single grain laser luminescence (SGLL) measurements using a novel automated reader. Nuclear Instruments and Methods in Physics Reseach B 155, 506-514.

Fàbiàn, S.A., Kovàcs, J., Varga, G., Sipos, G., Horvàth, Z., Thamo_Bozso, E., Toth, G., 2014. Distribution of relict permafrost features in the Pannonian Basin, Hungary. Boreas, Vol. 43, pp. 722-732.

Feray, P., 2009. Feignies (59), « Les Mottes », « Queue Bizenne » et « Grand Bray » : Extension de la zone d'activité du Parc de Grévaux les Guides. 51 pp. Rapport Final d'Opération, diagnostic archéologique, Inrap, Amiens.

Frechen, M., Van Vliet-Lanoë, B., Van den Haute, P., 2001. The Upper Pleistocene loess record at Harmignies/Belgium - High resolution terrestrial archive of climate forcing. Palaeogegraphy, Palaeoclimatology, Palaeoecology 173, 175-195.

French, H.M., Demitroff, M., Forman, S.L., 2003. Evidence for Late-Pleistocene Permafrost in the New Jersey Pine Barrens (Latitude 39°N), Eastern USA. Permafrost and Periglacial Processes 14, 259-274.

Galbraith, R.F., Green, P.F., 1990. Estimating the component ages in a finite mixture. International Journal of Radiation Applications and Instrumentation. Part D. Nuclear Tracks and Radiation Measurements 17, 197-206.

Galbraith, R.F., Laslett, G.M., 1993. Statistical models for mixed fission track ages. Nuclear Tracks and Radiation Measurements 21, 459-470.

Galbraith, R.F., Roberts, R.G., Laslett, G.M., Yoshida, H., Olley, J.M., 1999. Optical dating of single and multiple grains of quartz from Jinmium Rock Shelter, Northern Australia: Part I, Experimental design and statistical models. Archaeometry 41, 339-364.

Guérin, G., Mercier, N., Adamiec, G., 2011. Dose-rate conversion factors: update. Anc.TL, 29, 5-8.

Guhl, A., Bertran, P., Fitzsimmons, K.E., Zielhofer, C., 2013. Optically stimulated luminescence (OSL) dating of sand-filled wedges structures and their alluvial host sediments from Jonzac, SW France. Boreas 42, 317-332.

Huijzer, B., Vandenberghe, J., 1998. Climatic reconstruction of the Weichselian Pleniglacial in northwestern and central Europe. Journal of Quaternary Science, 13(5), 391–417.

Isarin, R., Huijzer, B., van Huissteden, K., 1998. Time-slice oriented multiproxy database (MPDB) for palaeoclimatie reconstruction. National Snow and Ice Data Center, University of Boulder, Colorado. http://nsidc.org/data/ggd248.html

Kadereit, A., Kind, C.J., Wagner, G.A., 2013. The chronological position of the Lohne Woil in the Nussloch loess section – re-evaluation for a European loess-marker horizon. Quaternary Science Reviews 59, 67-89.

Kasse, C., 2002. Sandy aeolian deposits and environments and their relation to climate during the Last Glacial Maximum and Lateglacial in northwest and central Europe. Progress in Physical Geography 26, 4, 507-532.

Kasse, C., Vandenberghe, J., 1998. Topographic and drainage control on Weichselian ice-wedge and sand-wedge formation, Vennebrügge, German–Dutch border. Permafrost and Periglacial Processes 9, 95–106.

Kasse, C., Vandenberghe, D., de Corte, F., van den Haute, P., 2007. Late Weichselian fluvio-aeolian sands and coversands of the type locality Grubbenvorst (southern Netherlands): sedimentary environments, climate record and age. Journal of Quaternary Science 22, 7, 695–708.

Kjaer, K.H., Lagerlun, E., Adrielsson, L., Thomas, P.J., Murray, A., Sandgren, P., 2006. The first independent chronology of Middle and Late Weichselian sediments from southern Sweden and the island of Bornholm. GFF, 128, 209-220.

Kolstrup, E., 2004. Stratigraphic and Environmental Implications of a large ice-wedge cast at Tjaereborg, Denmark. Permafrost and Periglacial Processes, 15, 31-40.

Kolstrup, E., 2007. OSL dating in palaeoenvironmental reconstructions. A discussion from a user's perspective. Estonian Journal of Earth Sciences, 56, 157-166.

Kolstrup, E., Mejdhal, V., 1986. Three frost wedge casts from Jutland (Denmark) and TL dating of their infill. Boreas 15, 311-321.

Kovàcs, J., Fàbiàn, S.A., Schweitzer, F., Varga, G., 2007. A relict sand-wedge polygon site in north-central Hungary. Permafrost and Periglacial Procecesses. 18, 379-384.

Kreutzer, S., Lauer, T., Meszner, S., Krbetschek, M.R., Faust, D., Fuchs, M., 2012. Chronology of the Quaternary profile Zeuchfeld in Saxony-Anhalt / Germany – a preliminary luminescence dating study. Zeitschrift für Geomorphologie fast track, 1–21.

Lautridou, J.P., 1985. Le cycle périglaciaire pléistocène en Europe du nord-ouest et plus particulièrement en Normandie. Thèse d'Etat, Université de Caen, 487 pp.

Lécolle, F., 1989. Le cours moyen de la Seine au Pléistocène moyen et supérieur. Thèse, Caen et Université de Rouen, 549 pp.

Lenoble, A., Bertran, P., Mercier, N., Sitzia L., 2012. Le site du Lac Bleu et la question de l'extension du pergélisol en France au Pléistocène supérieur. Quaternaire continental d'Aquitaine : un point sur les travaux récents. Livret-guide de l'excursion AFEQ-ASF 2012, Université de Bordeaux, AFEQ, 107-121.

Locht, J. L., Antoine, P., Auguste, P., Bahain, J.J., Debeham, N., Falguères, C., Farkh, S., Tissoux, H., 2006. La séquence lœssique Pléistocène supérieur de Savy (Aisne, France): stratigraphie, datations et occupations paléolithiques. Quaternaire, 17, 269–275.

Maarleveld, G.C., 1976. Periglacial phenomena and the mean annual air temperature during the last glacial time in The Netherlands. Biuletyn Periglacjalny, 26, 57–78.

Martin, L., Incerti, S., Mercier, N., 2015a. DosiVox : a Geant 4-based software for dosimetry simulations relevant to luminescence and ESR dating techniques. Ancient TL 33 n°1, 1-10.

Martin, L., Mercier, N., Incerti, S., Lefrais, Y., Pecheyran, C., Guérin, G., Jarry, M., Bruxelles, L., Bon, F., Pallier, C., 2015b. Dosimetric study of sediments at the Beta dose rate scale : characterization and modelization with the DosiVox software. Radiation Measurement 81, 134-141.

Mackay, J.R., 1993. Air temperature, snow cover, creep of frozen ground, and the time of ice-wedge cracking, western Arctic coast. Canadian Journal of Earth Sciences, 30 (8), 1720-1729.

Mejdhal, V., 1979. Thermoluminescence dating: Beta-dose attenuation in quartz grains. Archaeometry 21, 61-72.

Meszner, S., Kreutzer, S., Fuchs M., Faust, D., 2013. Late Pleistocene landscape dynamics in Saxony, Germany: Paleoenvironmental reconstruction using loess-paleosol sequences. Quaternay International, 296, 94-107.

Michel, J. P., 1969. Divers types de phénomènes périglaciaires et leur répartition dans les alluvions quaternaires de la Seine et de ses affluents. Supplément du Bulletin de l'Association Française pour l'Etude du Quaternaire 2, 721-735.

Michel, J.P., 1975. Périglaciaires des environs de Paris. Biuletyn Peryglacjalny, 24, 259-352.

Moine, O., Antoine, P., Deschodt, L., Sellier-Segard, N., 2011. Enregistrements malacologiques à haute résolution dans les loess et les gleys de toundra du Pléniglaciaire weichsélien supérieur: premiers exemples du nord de la France. Quaternaire 22, 307-325.

Murray, A.S., Wintle, A.G., 2000. Luminescence dating of quartz using an improved single- aliquot regenerative-dose protocol. Radiation Measurements 32, 57-73.

Murray, A.S., Wintle, A.G., 2003. The single aliquot regenerative dose protocol: Potential for improvements in reliability. Radiation Measurements, 37, 377-381.

Murton, J.B., 2013. Permafrost and Periglacial Features. Ice Wedges and Ice-Wedge Casts. In Encyclopedia of Quaternary Science (Second Edition), Elsevier, Amsterdam, 436-451.

Murton, J.B., Worsley, P., Gozdzik, J., 2000. Sand veins and wedges in cold Aeolian environments. Quaternary Science Reviews, 19 (9), 899-922.

Olley, J., Caitcheon, G., Murray, A., 1998. The distribution of apparent dose as determined by optical stimulated luminescence in small aliquots of fluvial quartz: Implications for dating young sediments. Quaternary Geochronology, 17, 1033-1040.

Péwé, T.L., 1966. Palaeoclimatic significance of fossil ice wedges. Biuletyn Peryglacjalny, 5, 65-72.

Ponel, P., Gandouin, E., Russell Coope, G., Andrieu-Ponel, V., Guiter, F., Van Vliet-Lanoë, B., Franquet, E., Brocandel, M., Brulhet, J., 2007. Insect evidence for environmental and climate changes from Younger Dryas to Sub-Boreal in a river floodplain at St-Momelin (St-Omer basin, northern France), Coleoptera and Trichoptera. Palaeogepgraphy, Palaeoclimatology, Palaeoecology 245, 483-504.

Prescott, J.R., Hutton, J.T., 1994. Cosmic-ray contributions to dose-rates for luminescence and ESR dating – Large depths and long-term time variations. Radiation Measurements 23, 497-500.

Rasmussen, S. O., Bigler, M., Blockley, S. P., Blunier, T., Buchardt, S. L., Clausen, H. B., Cvijanovic, I., Dahl-Jensen, D., Johnsen, S. J., Fischer, H., Gkinis, V., Guillevic, M., Hoek, W. Z., Lowe, J. J., Pedro, J., Popp, T. J., Seierstad, I. K., Steffensen, J. P., Svensson, A., Vallelonga, P. T., Vinther, B. M., Walker, M. J. C., Wheatley, J. J, Winstrup, M., 2014. A stratigraphic framework for abrupt climatic changes during the Last Glacial period based on three synchronized Greenland ice-core records: refining and extending the INTIMATE event stratigraphy. Quaternary Science Reviews, 106, 14-28.

Readhead, M.L., 2002. Absorbed dose fraction for 87Rb beta particles. Anc. TL 20, 25-29.

Renssen, H., Isarin, R.F.B., 1998. Surface temperature in NW Europe during the Younger Dryas: AGCM simulation compared with climate reconstructions. Climate Dynamics, 14, 33-44.

Roberts, R.G., Galbraith, R.F., Yoshida, H., Laslett, G.M., Olley, J.M., 2000. Distinguishing dose populations in sediment mixtures: a test of optical dating procedures using mixtures of laboratory-dosed quartz. Radiation Measurements, 32, 459-465.

Sanchez-Goñi, M.F., Harrison S.P., 2010. Millennial-scale climate variability and vegetation changes during the LastGlacial: Concepts and terminology. Quaternary Science Reviews 29, 2823-2827.

Sellier, N., Coutard, S., 2007. Données récentes sur le Paléolithique moyen de l'Aisne : une occupation du Weichselien ancien à Courmelles. Revue archéologique de Picardie 3-4, 5-16.

Sommé, J., Tuffreau., A., 1971. Stratigraphie du Pléistocène récent et Moustérien de Tradition Acheuléenne à Marcoing (Cambresis – nord de la France). Bulletin de l'Association Française pour l'Etude du Quaternaire 2, 57-74.

Simonis, D., Hense, A., Litt, T., 2012. Reconstruction of late Glacial and Early Holocene near surface temperature anomalies in Europe and their statistical interpretation. Quaternary International, 274, 233-250.

Sitzia, L., Bertran, P., Bahain, J.J., Bateman, M.D., Hernandez, M., Garon, H., De Lafontaine, G., Mercier, N., Leroyer, C., Queffelec A., Voinchet, P., 2015. The quaternary coversands of southwest France. Quaternary Science Reviews, 124, 84-105.

Tricart, J., 1956. Carte des phénomènes périglaciaires quaternaires en France. Mémoire pour servir à l'explication de la carte géologique détaillée de la France. Ministère de l'Industrie et du Commerce: Paris.

Vandenberghe, D., De Corte, F., Buylaert, J.-P., Kucera, J., Van Den Haute, P., 2008. On the internal radioactivity in quartz. Radiation Measurements, 43, 771-775.

Vandenberghe, J., 1983. Ice-wedge casts and involutions as permafrost indicators and their stratigraphic position in the Weichselian. Proceedings of the 4th International Conference on Permafrost, Fairbanks, Alaska, 1, 1298-1302.

Vandenberghe, J., Lowe, J., Coope, G. R., Litt, T., & Zöller, L., 2004. Climatic and environmental variability in the Mid-Latitude Europe sector during the last interglacial-glacial cycle. In R. Battarbee, F. Gasse, & C. Stickley (Eds.), Past Climate Variability through Europe and Africa: PEPIII Conference Proceedings (pp. 393-416). Dordrecht: Kluwer.

Vandenberghe, J., French, H., Gorbunov, A., Marchenko, S., Velichko, A.A., Jin, H., Cui, Z., Zhang, T., Wan, X., 2014. The Last permafrost Maximum (LPM) map of the Northern Hemisphere: permafrost extent and mean annual air temperatures, 25-17 ka. Boreas, 43, 652–666.

Van Vliet-Lanoë, B., Hallégouët, B., 2001. European permafrost at the LGM and at its maximal extent. The geological approach. In Permafrost Response on Economic Development, Environmental Security and Natural Resources, Paepe R, Melnikov V (eds). Kluwer Academic Publishers: Dordrecht, 195–213.

Wanner, H., Solomina, O., Grosjean, M., Ritz, S.P., Markéta, J., 2011. Structure and origin of Holocene cold events. Quaternary Science reviews, 30, 3109-3123.

Williams, R.B.G., 1968. Periglacial climate and its relation to landforms: a study of southern and eastern England during the Last Glacial Period. PhD Thesis, University of Cambridge.

Wojdyr, M.J., 2010. Fityk: a general-purpose peak fitting program. Journal of Applied Crystallography 43, 1126-1128.

Wolfe, S.A., Morse, P.D., Kokelj, S.V., Neudorf, C.M., Lian, O.B., 2016. Contrasting environments of sand wedge formation in discontinuous permafrost, Great Slave High Boreal Plains, Northwest Territories, Canada. Abstracts, 11th international conference on permafrost, 20-24 June 2016, Potsdam, Germany, 112.

Figure captions:

Figure 1: Spatial distribution of the relict periglacial wedge features in France and Northern Europe with zooms on A) Loire valley and B) Northern Aquitaine. OSL dating was carried out on the numbered features, the ones dated therein are highlighted with a black square. 1 Challans ; 2 Durtal ; 3 La Flèche ; 4, 5, 6 La-Chapelle-aux-Choux ; 7 Olivet ; 8 Sainte-Geneviève-des-Bois ; 9 Jau-Dignac ; 10 Jonzac (Guhl et al., 2013) ; 11 Cussac-Fort-Médoc ; 12 Saint-André-de-Cubzac ; 13 Salaunes ; 14, 15 Mérignac ; 16 Pessac Cap-de-Bos, 17 Léognan Lac Bleu (Lenoble et al., 2012). Northern Europe data was extracted from Isarin et al. (1998) and France data from Andrieux et al. (2016a, 2016b). The permafrost limits (thick, fine, and doted lines) were drawn on figure 1A according to the modelled LGM isotherms provided by K. Saito (Saito et al., 2013) that best fit with the mapped periglacial features.

Figure 2: Relict sand-wedges in A) Mérignac (Chronopost), B) Cussac-Fort-Médoc (Parcelle Lagrange), C) and D) La Chapelle-aux-Choux, E) Saint-Christophe-du-Ligneron (Challans)

Figure 3: Examples of probability density functions (pdf) plotted for the single grain samples Shfd13040 and Shfd14022 with the individual grain results above (Black) and mean (grey) showing multiple De components. Overdispersion values (OD) were calculated as per Galbraith et al., (1999), skewness (Sk) as per Bailey and Arnold (2006). N = number of measured grains.

Figure 4: Probability density of the FMM ages (blue line) and FMM estimates of the Loire valley (white) and Northern Aquitaine (black), plotted together with the NGRIP δO^{18} data over the last 100 ka tuned to the revised Greenland Ice Core Chronology proposed by Rasmussen et al. (2014). The distribution of the probability density function was adjusted to a combination of Gaussian functions (red lines) using the software Fityk 0.9.8 (Wojdyr, 2010). The respective contribution of each Gaussian function to the dataset was expressed as a percentage of the total. The goodness of fit was assessed using R^2, which reached almost unity (R^2=0.9999). Blue boxes in the NGRIP curve and over the age estimates represent the Full Width at Half Maximum (FWHM) of each Gaussian function fitted. Grey shading represent the interglacial and greenland interstadials and vertical black dashed lines show the limits of each MIS.

Figure 5: Probability density function of the ages calculated with A) CAM, B) MAM, and C) FMM.

Figure 6: Representative case study of two wedges sampled A) Mérignac (Chronopost) and B) Sainte-Genevieve-des-bois (Les Bézards). OSL ages are calculated from FMM components which contribution in the sample is shown in percentage. Coloured circles show the overlap of ages between the samples and their belonging to an age cluster.

Figure 7 : Probability density of the sand wedge ages in Northern Aquitaine compared with the aeolian records from southwest France (Sitzia et al., 2015) and the insolation in June and December at 60°N (Berger, 1978). Interstadials and the Holocene are illustrated by grey shading and light grey indicates cold sub-events (Rasmussen et al., 2014).

Table captions:

Table 1: Location of the studied features

Area	Site	Sample	Lab code	Latitude (°)	Longitude (°)	Altitude (m a.s.l.)
Northern Aquitaine	Salaunes - Château Montgaillard	Montg13.1	Shfd14011	44.935	-0.821	49
		Montg13.2	Shfd14012			
		Montg13.3	Shfd14013			
		Montg13.4	Shfd14014			
	Cussac-Fort Médoc - Parcelle Lagrange	Cu13.1	Shfd14021	45.114	-0.75	38
		Cu13.2	Shfd14022			
		Cu13.3	Shfd14023			
		Cu13.4	Shfd14024			
		Cu13.5	Shfd14025			
		Cu13.6	Shfd14026			
	Mérignac - Chronopost	MC13.1	Shfd14015	44.827	-0.689	47
		MC13.2	Shfd14016			
		MC13.3	Shfd14017			
		MC13.4	Shfd14018			
		MC13.5	Shfd14019			
		Chronopost 1	Shfd12099-1			
	Saint-André-de-Cubzac	St André 2	Shfd12098-1	45.01	0.26	52
Loire valley	La Chapelle-aux-Choux	CAH1.1	Shfd15076	47.617	0.211	69
		CAH2.1	Shfd15077			
		CAH2.2	Shfd15078			
		CAH2.3	Shfd15079			
		CAH4.1	Shfd15083			
		CAH4.2	Shfd15084			
	Olivet	O1	Shfd15085	47.815	1.927	114
		O2	Shfd15086			
	Sainte-Geneviève-des-Bois - Les Bézards	B1	Shfd15087	47.81	2.742	145
		B2	Shfd15088			
		B3	Shfd15089			
		B4	Shfd15090			
	Durtal	Durtal	Shfd14028	47.66	-0.231	39
		Durtal 3	Shfd13040			

	Saint-Christophe-du-Ligneron - Challans	Challans 2	Shfd14020	46.8	1.76	32
	La Flèche - La Louverie	Lou3	Shfd14027	47.685	-0.01	34

Table 2: Elemental and associated data used to calculate OSL sample dose rates.

Lab code	K (%)	U (ppm)	Th (ppm)	Rb (ppm)	Alpha(uGy/ka)	Beta (uGy/ka)	Gamma (uGy/ka)	O. (m)	Cosmic (uGy/ka)	Water content (%)	Dose rate (µGy/a)
Shfd14011	0.4 ± 0.02	0.87 ± 0.087	3.7 ± 0.37	26 ± 2.6	22 ± 4	589 ± 40	337 ± 22	1.1	182 ± 9	8.7 ± 5	1130 ± 46
Shfd14012	0.4 ± 0.02	0.67 ± 0.067	3 ± 0.3	21.8 ± 2.18	20 ± 4	563 ± 39	304 ± 20	1.1	182 ± 9	3.8 ± 5	1070 ± 44
Shfd14013	0.4 ± 0.02	0.67 ± 0.067	3 ± 0.3	19.9 ± 1.99	20 ± 3	552 ± 38	305 ± 20	1	184 ± 9	3.7 ± 5	1062 ± 44
Shfd14014	0.4 ± 0.02	0.63 ± 0.063	2.8 ± 0.28	21.1 ± 2.11	19 ± 2	535 ± 37	283 ± 18	0.85	188 ± 9	6 ± 5	1026 ± 42
Shfd14021	0.4 ± 0.02	0.61 ± 0.061	2 ± 0.2	19 ± 1.9	18 ± 4	531 ± 37	258 ± 17	0.61	193 ± 10	1.8 ± 5	1001 ± 42
Shfd14022	0.5 ± 0.025	1.73 ± 0.173	4.2 ± 0.42	27.1 ± 2.71	28 ± 3	802 ± 55	487 ± 31	0.61	193 ± 10	5.5 ± 5	1510 ± 48
Shfd14023	0.4 ± 0.02	0.59 ± 0.059	2 ± 0.2	16.6 ± 1.66	18 ± 3	516 ± 37	257 ± 16	0.61	193 ± 10	1.4 ± 5	984 ± 32
Shfd14024	0.4 ± 0.02	0.72 ± 0.072	1.9 ± 0.19	16.2 ± 1.62	18 ± 3	520 ± 37	263 ± 17	0.61	193 ± 10	2.5 ± 5	995 ± 41
Shfd14025	0.5 ± 0.025	0.61 ± 0.061	2.4 ± 0.24	20.4 ± 2.04	19 ± 4	623 ± 44	302 ± 19	0.61	193 ± 10	1.6 ± 5	1138 ± 49
Shfd14026	0.6 ± 0.03	0.75 ± 0.075	2.9 ± 0.29	29.7 ± 2.97	21 ± 4	770 ± 54	359 ± 23	0.61	193 ± 10	3 ± 5	1343 ± 59
Shfd14015	0.4 ± 0.02	0.99 ± 0.099	4.2 ± 0.42	22.3 ± 2.23	22 ± 2	501 ± 34	318 ± 20	0.9	187 ± 9	20.4 ± 5	1221 ± 50
Shfd14016	0.5 ± 0.03	1.04 ± 0.104	5.2 ± 0.52	27.7 ± 2.77	24 ± 4	623 ± 42	389 ± 25	0.9	187 ± 9	18.5 ± 5	1357 ± 56
Shfd14017	0.4 ± 0.02	0.88 ± 0.088	4.3 ± 0.43	24.6 ± 2.46	22 ± 3	552 ± 37	340 ± 22	0.9	187 ± 9	14.1 ± 5	1189 ± 48
Shfd14018	0.4 ± 0.02	0.71 ± 0.071	3.1 ± 0.31	20.7 ± 2.07	19 ± 4	455 ± 31	257 ± 16	0.9	187 ± 9	19.3 ± 5	1060 ± 43
Shfd14019	0.4 ± 0.02	0.85 ± 0.085	3.7 ± 0.37	22.3 ± 2.23	20 ± 2	474 ± 32	284 ± 18	0.9	187 ± 9	21.2 ± 5	1139 ± 46
Shfd12099	0.3 ± 0.02	0.88 ± 0.088	3.4 ± 0.34	24.1 ± 2.41	23 ± 2	567 ± 51	336 ± 22	2	161 ± 8	5.2 ± 5	1029 ± 42
Shfd12098	1.2 ± 0.06	0.95 ± 0.095	3.8 ± 0.38	53.8 ± 5.38	23 ± 2	1311 ± 95	535 ± 34	1.8	165 ± 8	7.8 ± 5	2034 ± 102
Shfd15076	0.4 ± 0.02	0.87 ± 0.087	4.4 ± 0.44	27.8 ± 2.78	24 ± 2	639 ± 43	382 ± 25	1.2	180 ± 9	5.6 ± 5	1225 ± 50
Shfd15077	0.5 ± 0.03	1.42 ± 0.142	7.1 ± 0.71	46.1 ± 4.61	30 ± 2	825 ± 55	518 ± 33	0.6	196 ± 10	15.16 ± 5	1569 ± 66
Shfd15078	0.4 ± 0.02	1.1 ± 0.11	5.6 ± 0.56	40.5 ± 4.05	26 ± 2	702 ± 47	423 ± 27	0.6	196 ± 10	12.29 ± 5	1347 ± 56
Shfd15079	0.4 ± 0.02	0.99 ± 0.099	5.7 ± 0.57	46.1 ± 4.61	26 ± 2	740 ± 50	426 ± 28	0.8	190 ± 10	10.62 ± 5	1382 ± 58
Shfd15083	0.2 ± 0.01	0.56 ± 0.056	2 ± 0.2	7.2 ± 0.72	18 ± 3	303 ± 22	203 ± 13	0.6	196 ± 10	2 ± 5	720 ± 27
Shfd15084	0.2 ± 0.01	0.44 ± 0.044	1.5 ± 0.15	6.6 ± 0.66	16 ± 2	272 ± 19	166 ± 11	0.9	188 ± 9	2.5 ± 5	642 ± 24
Shfd15085	2.5 ± 0.13	1.25 ± 0.125	4.5 ± 0.45	110 ± 11	27 ± 2	2789 ± 211	962 ± 64	1	187 ± 9	1.4 ± 5	3689 ± 202
Shfd15086	2.7 ± 0.14	1.64 ± 0.164	6.5 ± 0.65	126 ± 12.6	33 ± 2	2969 ± 218	1094 ± 72	1.4	177 ± 9	5.5 ± 5	4483 ± 241
Shfd15087	2.4 ± 0.12	1.38 ± 0.138	7.7 ± 0.77	119 ± 11.9	34 ± 2	2713 ± 197	1051 ± 68	1.5	175 ± 9	5.5 ± 5	3973 ± 209

Shfd15088	2.2 ± 0.11	1.36 ± 0.136	7.1 ± 0.71	110 ± 11	31 ± 2	2343 ± 171	917 ± 59	1.2	183 ± 9	10.5 ± 5	3695 ± 193
Shfd15089	1.2 ± 0.06	1.47 ± 0.147	8.1 ± 0.81	77.7 ± 7.77	35 ± 2	1589 ± 109	772 ± 49	1	188 ± 9	8.2 ± 5	2583 ± 121
Shfd15090	2.5 ± 0.13	1.31 ± 0.131	7 ± 0.7	121 ± 12.1	32 ± 2	2779 ± 204	1038 ± 68	1	188 ± 9	5.3 ± 5	4037 ± 215
Shfd14028	0.3 ± 0.02	0.5 ± 0.05	2.3 ± 0.23	14.7 ± 1.47	18 ± 3	320 ± 25	228 ± 15	0.8	189 ± 9	3.9 ± 5	755 ± 30
Shfd13040	0.2 ± 0.01	0.45 ± 0.045	1.6 ± 0.16	14.1 ± 1.41	16 ± 2	310 ± 22	165 ± 11	1.1	181 ± 9	5.6 ± 5	673 ± 25
Shfd14020	0.8 ± 0.04	1.24 ± 0.124	5.3 ± 0.53	43.4 ± 4.34	28 ± 2	1051 ± 73	543 ± 35	1.1	181 ± 9	7.2 ± 5	1803 ± 81
Shfd14027	0.2 ± 0.01	0.42 ± 0.042	1.8 ± 0.18	11.7 ± 1.17	16 ± 3	236 ± 19	178 ± 11	0.6	194 ± 10	1.6 ± 5	626 ± 24

Table 3: Finite Model Mixture (FMM) ages in comparison with the estimates calculated from the Central Age Model (CAM) and Minimum Age Model (MAM)

Site	Lab code	Central Age Model		Minimum Age Model		Finite Mixture Model		
		De (Gy)	Age (ka)	De (Gy)	Age (ka)	De Component (Gy)	De Component (%)	Age (ka)
Salaunes - Château Montgaillard	Shfd14011	27.11 ± 1.56	23.98 ± 1.69	21.5 ± 1.27	19.02 ± 1.37	17.5161 ± 1.513	25	15.58 ± 1.49
						29.9071 ± 1.708	57	26.46 ± 1.86
						52.324 ± 4.285	17	46.29 ± 4.24
	Shfd14012	16.19 ± 0.92	15.13 ± 1.06	15.29 ± 0.58	14.29 ± 0.81	16.6355 ± 0.541	74	15.55 ± 0.82
						34.8896 ± 2.547	18	32.61 ± 2.74
	Shfd14013	16.68 ± 0.85	15.71 ± 1.03	16.82 ± 0.31	15.84 ± 0.72	16.401 ± 0.709	72	15.45 ± 0.92
						27.092 ± 3.021	17	25.52 ± 3.03
	Shfd14014	20.88 ± 0.92	20.36 ± 1.23	20.09 ± 1.16	19.59 ± 1.39	8.872 ± 1.189	10	8.65 ± 1.21
						21.4495 ± 0.719	76	20.91 ± 1.11
						40.6771 ± 3.384	14	39.66 ± 3.68
Cussac-Fort Médoc - Parcelle Lagrange	Shfd14021	56.09 ± 3.51	56.05 ± 4.22	41.97 ± 1.95	41.94 ± 2.63	30.5052 ± 1.968	27	30.49 ± 2.35
						72.4853 ± 2.392	73	72.44 ± 3.87
	Shfd14022	27.87 ± 1.88	18.45 ± 1.37	22.69 ± 0.73	15.02 ± 0.68	22.51 ± 0.887	63	14.9 ± 0.75
						53.684 ± 2.443	37	35.55 ± 2.21
	Shfd14023	15.5 ± 0.7	15.75 ± 0.97	16.08 ± 0.31	16.33 ± 0.76	14.8822 ± 0.588	80	15.12 ± 0.77
						22.4762 ± 2.434	18	22.83 ± 2.65
	Shfd14024	15.81 ± 0.98	15.89 ± 1.19	14.3 ± 0.75	14.37 ± 0.97	15.0239 ± 0.793	62	15.1 ± 1.02
						25.5927 ±	30	25.72 ±

						2.111		2.38
	Shfd14025	17.37 ± 0.91	15.27 ± 1.04	17.68 ± 0.29	15.54 ± 0.72	18.3634 ± 0.562 56.3969 ± 4.67	73 11	16.14 ± 0.86 49.58 ± 4.64
	Shfd14026	26.01 ± 2.38	19.36 ± 1.97	20.01 ± 0.81	14.89 ± 0.9	15.0251 ± 1.127 24.4409 ± 1.347 58.2539 ± 4.905 156.2825 ± 13.925	25 37 16 22	11.18 ± 0.97 18.19 ± 1.29 43.36 ± 4.13 116.33 ± 10.91
Mérignac-Chronopost	Shfd14015	20.83 ± 1.38	20.27 ± 1.57	14.64 ± 0.69	14.25 ± 0.88	8.4222 ± 0.824 19.2245 ± 1.321 30.4879 ± 1.747	13 39 41	8.18 ± 0.87 18.71 ± 1.48 29.67 ± 2.07
	Shfd14016	17.3 ± 0.93	13.93 ± 0.95	14.48 ± 0.51	11.84 ± 0.64	14.7663 ± 0.534 29.001 ± 1.529	68 32	12.08 ± 0.66 23.72 ± 1.58
	Shfd14017	16.41 ± 0.77	14.9 ± 0.92	12.51 ± 0.61	11.36 ± 0.72	13.3105 ± 1.762 19.3465 ± 2.3	36 55	12.09 ± 1.67 17.57 ± 2.21
	Shfd14018	14.07 ± 0.68	15.33 ± 0.96	14.5 ± 0.20	15.8 ± 0.67	13.8868 ± 0.507 23.1301 ± 2.8843	84 13	15.13 ± 0.82 25.2 ± 3.3
	Shfd14019	14.92 ± 0.96	15.46 ± 1.17	11.78 ± 0.59	12.21 ± 0.79	7.4434 ± 0.913 17.2444 ± 0.607	17 79	7.71 ± 0.99 17.87 ± 0.95
	Shfd12099-2	18.98 ± 0.75	18.44 ± 1.05	17.72 ± 0.39	17.21 ± 0.8	17.6972 ± 0.676 28.9987 ± 2.329	65 22	17.19 ± 0.97 28.17 ± 2.54
Saint-André-de-Cubzac	Shfd12098-2	25.91 ± 1.17	12.74 ± 0.86	20.44 ± 0.80	10.05 ± 0.64	18.7443 ± 1.336 32.5813 ± 1.287	31 66	9.21 ± 0.81 16.02 ± 1.02

Site	Lab code	Central Age Model		Minimum Age Model		Finite Mixture Model		
		De (Gy)	Age (ka)	De (Gy)	Age (ka)	De Component (Gy)	De Component (%)	Age (ka)
La Chapelle-aux-Choux	Shfd15076	63.54 ± 3.03	51.86 ± 3.27	53.41 ± 2.69	43.59 ± 2.84	54.0867 ± 2.921 83.078 ± 4.81	46 45	44.14 ± 3.01 67.8 ± 4.82
	Shfd15077	94.8 ± 5.7	60.42 ± 4.42	60.98 ± 3	38.87 ± 2.51	47.8942 ± 3.7692 94.3216 ± 6.244	21 46	30.53 ± 2.73 60.12 ± 4.71

						176.7245 ± 11.027	33	112.64 ± 8.46
	Shfd15078	122.91 ± 8.11	91.22 ± 7.1	84.98 ± 4.53	63.07 ± 4.25	91.0753 ± 6.639 180.2477 ± 8.2192	36 53	67.59 ± 5.66 133.78 ± 8.22
	Shfd15079	113.09 ± 9.12	81.8 ± 7.44	64.96 ± 3.21	46.99 ± 3.05	60.8352 ± 4.417 125.3123 ± 8.421 220.7999 ± 13.182	21 43 31	44 ± 3.69 90.64 ± 7.18 159.71 ± 11.66
	Shfd15083	99.22 ± 8.19	137.81 ± 12.5	65.06 ± 3.93	90.36 ± 6.43	67.4209 ± 4.355 116.2007 ± 10.528 228.8668 ± 18.035	29 34 28	93.64 ± 7.01 161.39 ± 15.84 317.88 ± 27.76
	Shfd15084	53.62 ± 3.79	83.57 ± 6.7	31.67 ± 1.43	49.36 ± 2.91	25.4295 ± 2.2454 54.726 ± 2.501 113.4103 ± 10.037 216.1 ± 24.657	14 49 24 10	39.64 ± 3.81 85.3 ± 5.05 176.77 ± 17.01 336.82 ± 40.48
Olivet	Shfd15085	118.83 ± 8	29.97 ± 2.6	73.42 ± 3.39	18.52 ± 1.33	69.5658 ± 4.153 132.4353 ± 10.833 208.6423 ± 16.942	27 41 32	17.55 ± 1.43 33.4 ± 3.29 52.62 ± 5.16
	Shfd15086	112.92 ± 7.6	26.43 ± 2.28	83.81 ± 4.13	19.61 ± 1.43	48.236 ± 4.703 97.257 ± 5.68 176.3477 ± 8.288	12 40 47	11.29 ± 1.26 22.76 ± 1.81 41.27 ± 2.95
Sainte-Geneviève-des-Bois - Les Bézards	Shfd15087	103.4 ± 7.86	26.03 ± 2.41	75.38 ± 5.09	18.97 ± 1.63	69.475 ± 5.44 124.2104 ± 13.806 239.435 ± 15.016	42 31 28	17.49 ± 1.66 31.26 ± 3.62 60.27 ± 4.93
	Shfd15088	125.09 ± 11.83	36.01 ± 3.89	90.07 ± 5.65	25.93 ± 2.12	39.7643 ± 4.2667 90.2591 ± 10.569 203.9413 ± 10.707	12 26 62	11.45 ± 1.37 25.98 ± 3.33 58.71 ± 4.34
	Shfd15089	109.71 ± 10.71	42.47 ± 4.6	71.25 ± 5.28	27.58 ± 2.42	54.2115 ± 7.1722 102.8782 ± 9.382 208.1408 ± 12.988	19 39 38	20.98 ± 2.94 39.82 ± 4.08 80.57 ± 6.58

	Shfd15090	90.88 ± 10.09	22.51 ± 2.77	70.65 ± 5.95	17.5 ± 1.75	30.3856 ± 4.376 71.5037 ± 8.623 133.2005 ± 12.547 278.2291 ± 34.389	12 32 36 20	7.53 ± 1.16 17.71 ± 2.34 33 ± 3.57 68.92 ± 9.28
Durtal	Shfd14028	40.82 ± 2.39	54.06 ± 3.84	28.02 ± 1.16	37.1 ± 2.14	18.1332 ± 1.3274 40.3646 ± 1.954 64.0464 ± 4.221	14 51 32	24.01 ± 2 53.45 ± 3.36 84.81 ± 6.54
	Shfd13040-2	16.92 ± 0.74	25.15 ± 1.45	16.54 ± 0.46	24.58 ± 1.16	14.7938 ± 0.928 21.9162 ± 2.834 37.7118 ± 3.2319	56 27 13	21.99 ± 1.62 32.57 ± 4.39 56.05 ± 5.25
Saint-Christophe-du-Ligneron - Challans	Shfd14020	56.05 ± 2.01	31.08 ± 1.78	55.49 ± 2.56	30.77 ± 1.98	57.9666 ± 2.73 89.328 ± 11.371	79 12	32.14 ± 2.1 49.53 ± 6.68
La Flèche - La Louverie	Shfd14027	39.86 ± 2.02	63.71 ± 4.06	30.92 ± 1.32	49.42 ± 2.85	13.0501 ± 1.163 36.3304 ± 2.478 54.1907 ± 3.251	14 45 42	20.86 ± 2.03 58.07 ± 4.55 86.62 ± 6.18

Figure A1: Single-aliquot regenerative dose (SAR) OSL decay curves and dose response curves for a single grain of sample Shfd14022. The used signal and background intervals are highlighted in grey.

Figure A2: Dose-recovery preheat plateau test performed on three small aliquots at each temperature. The average values of the dose recovery (black) and the recycling ratio (white) are presented with standard deviation. The solid line indicates the ideal values.

Figure A3: Probability density functions (pdf, solid line) plotted for all samples with the individual grain results above (Black) and mean (dark grey), compared with the pdf (grey filled curv) of the same data without outliers. Overdispersion values (OD), and OD without outliers (C.OD) were calculated as per Galbraith et al., (1999), skewness (Sk) and Sk without outliers (C.Sk) as per Bailey and Arnold (2006). N = number of measured grains.

Figure A4: Single grain dose recovery results performed on samples Shfd14023 and Shfd14027 shown as radial plots of measured recovered dose on given dose (Dg). The shaded areas show the two sigma errors. OD = Overdispersion and N = number of grains.

Table A1: The Single-Aliquot Regenerative-dose (SAR) protocol used in this study

Step	**Treatment**
1	Give dose*
2	Pre-heat (160-220°C for 10s, heating at a rate of 2°C/s)
3	Stimulation of single grains with green laser light (90% power) for 1s at 125°C
4	Test dose
5	Cut-heat (160°C for 0s, heating at a rate of 2°C/s)
6	Stimulation of single grain with green laser light (90% power) for 1s at 125°C
7	Return to step 1

* The final dose given is equal to the first regeneration dose allowing the calculation of a recycling ratio. The third or fourth regeneration point is always 0 Gy allowing recuperation to be observed.

Highlights

- Single-grain OSL was performed on 33 samples taken from sand-wedges.
- Multiple phases of activity were identified within sand-wedges.
- Thermal contraction cracking occurred at least 11 times over the last 100 ka.
- Sand-wedges grew within deep-seasonal ground freezing during low insolation periods.
- Poor record of periglacial periods concomitant with low sand availability.

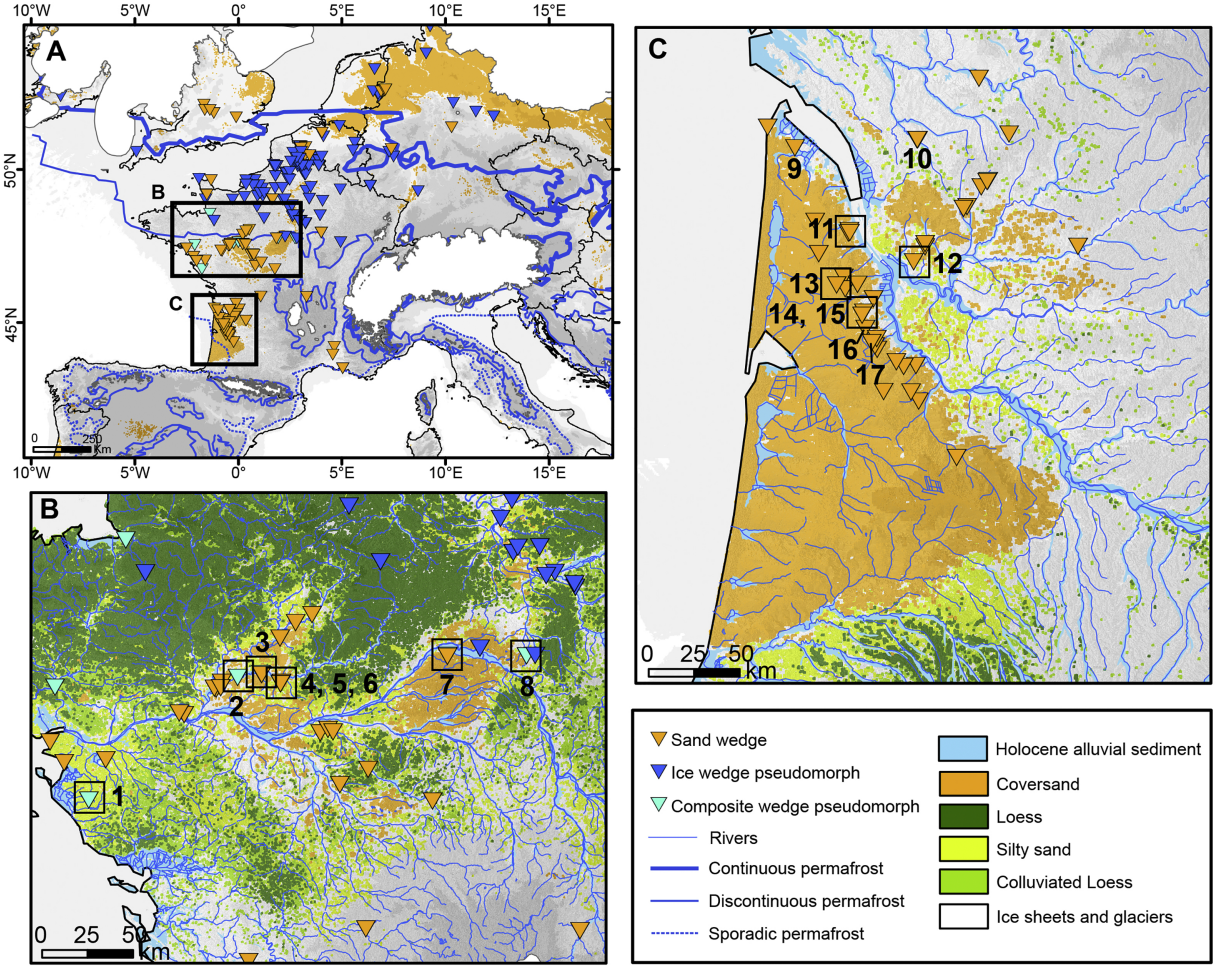
A
B
C
10°W
5°W
0°
5°E
10°E
15°E
50°N
45°N
0
250
km
B
1
2
3
4, 5, 6
7
8
0
25
50
km
C
9
10
11
12
13
14, 15
16
17
0
25
50
km
Sand wedge
Ice wedge pseudomorph
Composite wedge pseudomorph
Rivers
Continuous permafrost
Discontinuous permafrost
Sporadic permafrost
Holocene alluvial sediment
Coversand
Loess
Silty sand
Colluviated Loess
Ice sheets and glaciers

Figure 1

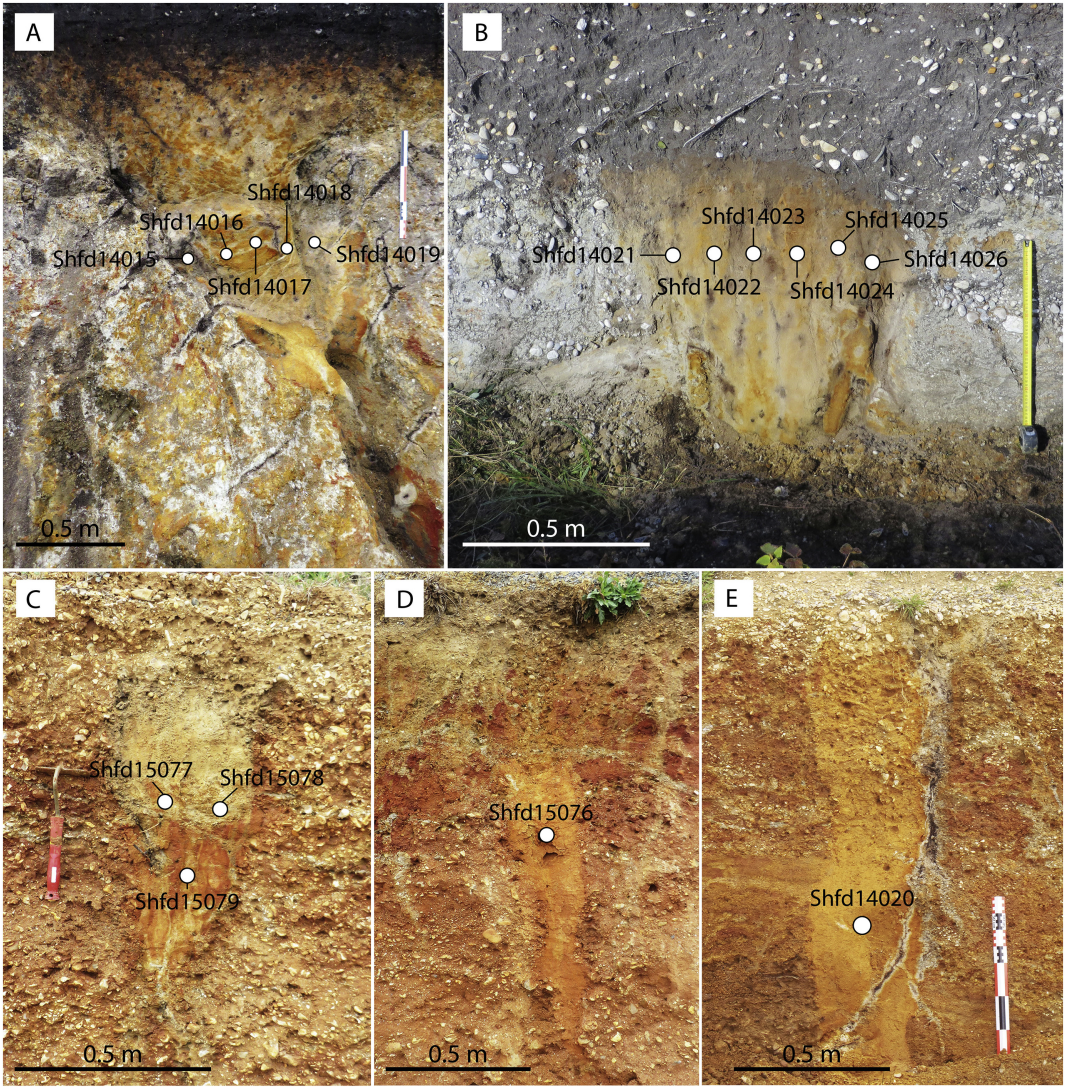
A
Shfd14018
Shfd14016
Shfd14015
Shfd14019
Shfd14017
0.5 m
B
Shfd14023
Shfd14025
Shfd14021
Shfd14026
Shfd14022
Shfd14024
0.5 m
C
Shfd15077
Shfd15078
Shfd15079
0.5 m
D
Shfd15076
0.5 m
E
Shfd14020
0.5 m

Figure 2

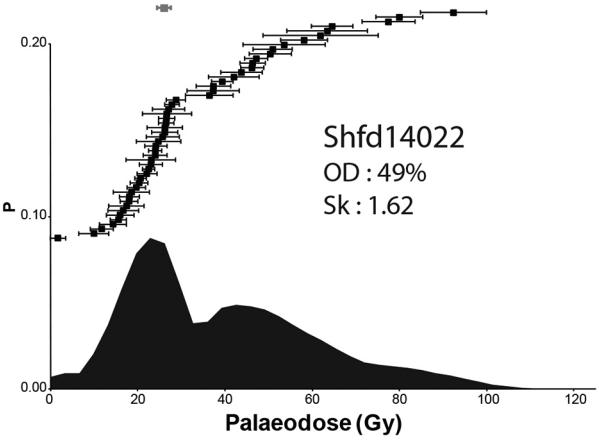
Shfd14022
OD : 49%
Sk : 1.62
P
Palaeodose (Gy)

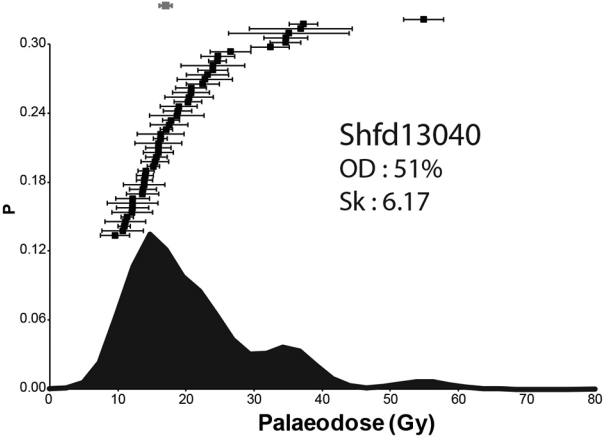
Shfd13040
OD : 51%
Sk : 6.17
P
Palaeodose (Gy)

Figure 3

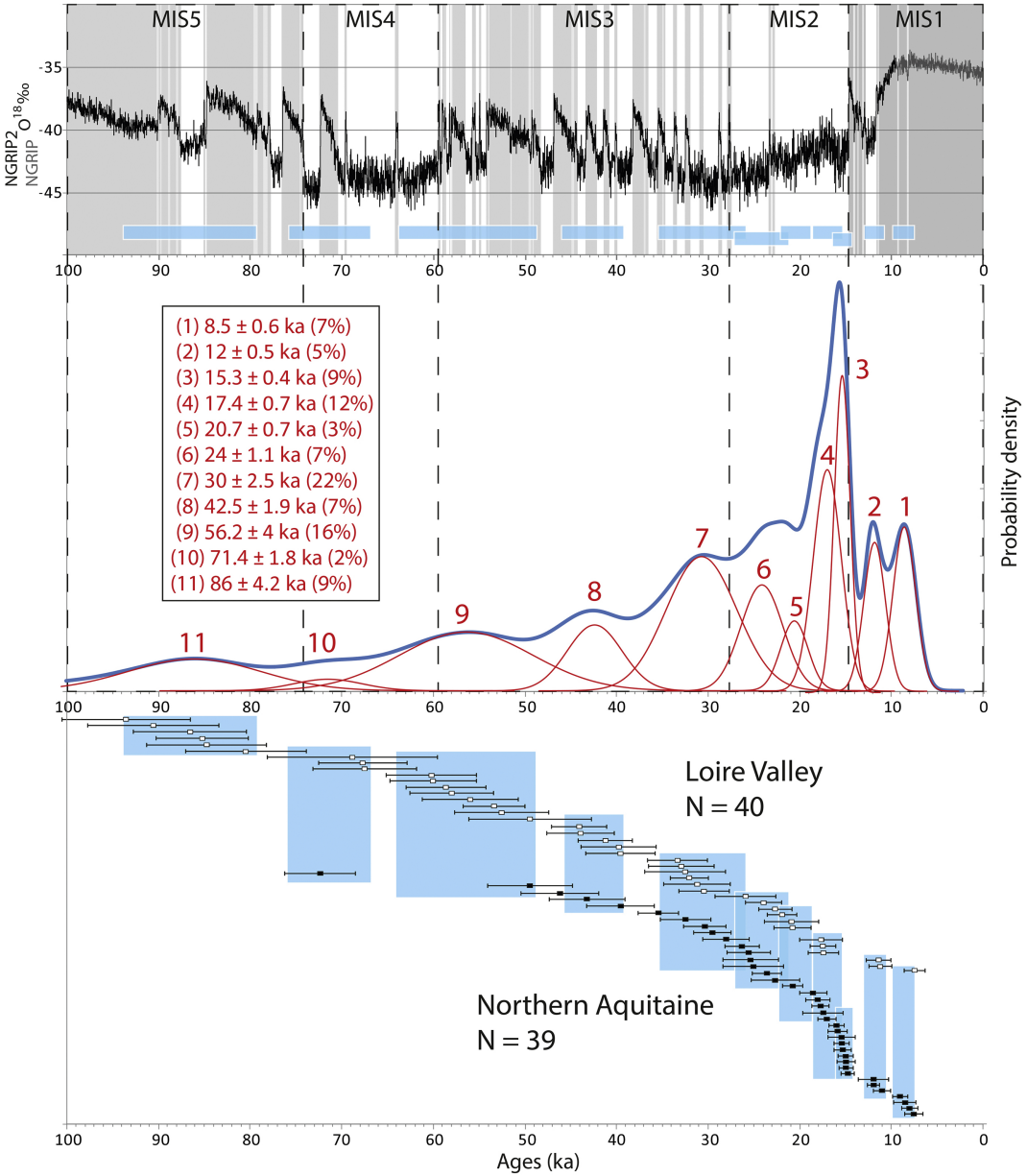
MIS5
MIS4
MIS3
MIS2
MIS1
NGRIP2 NGRIP O^{18}‰
-35
-40
-45
100
90
80
70
60
50
40
30
20
10
0
(1) 8.5 ± 0.6 ka (7%)
(2) 12 ± 0.5 ka (5%)
(3) 15.3 ± 0.4 ka (9%)
(4) 17.4 ± 0.7 ka (12%)
(5) 20.7 ± 0.7 ka (3%)
(6) 24 ± 1.1 ka (7%)
(7) 30 ± 2.5 ka (22%)
(8) 42.5 ± 1.9 ka (7%)
(9) 56.2 ± 4 ka (16%)
(10) 71.4 ± 1.8 ka (2%)
(11) 86 ± 4.2 ka (9%)
11
10
9
8
7
6
5
4
3
2
1
Probability density
Loire Valley
N = 40
Northern Aquitaine
N = 39
Ages (ka)

Figure 4

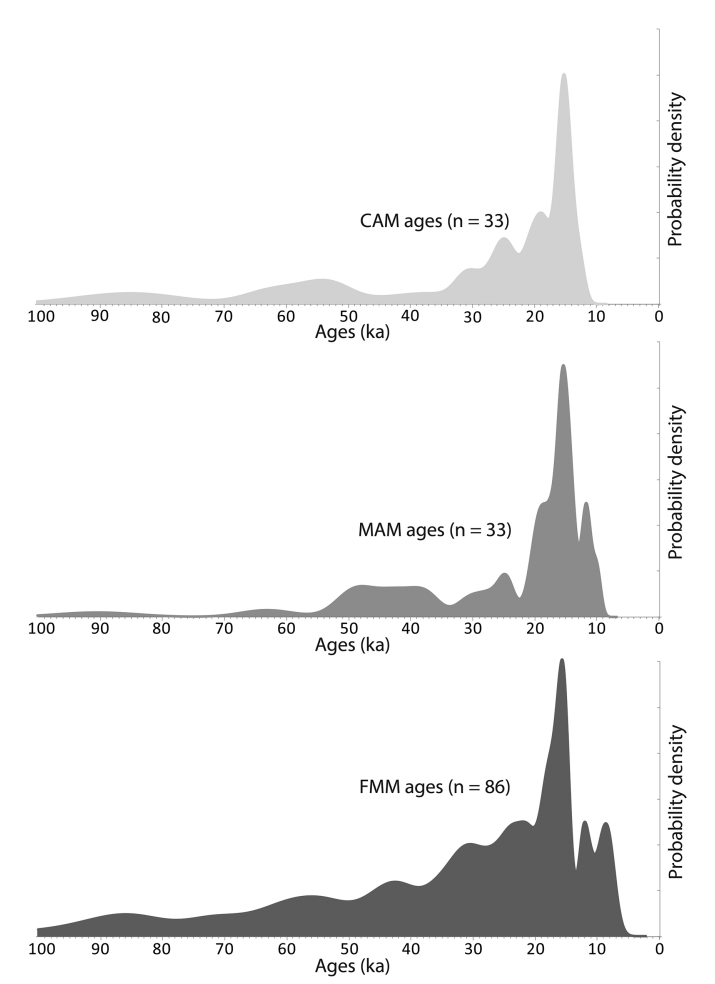
CAM ages (n = 33)
Probability density
100 90 80 70 60 50 40 30 20 10 0
Ages (ka)
MAM ages (n = 33)
Probability density
100 90 80 70 60 50 40 30 20 10 0
Ages (ka)
FMM ages (n = 86)
Probability density
100 90 80 70 60 50 40 30 20 10 0
Ages (ka)

Figure 5

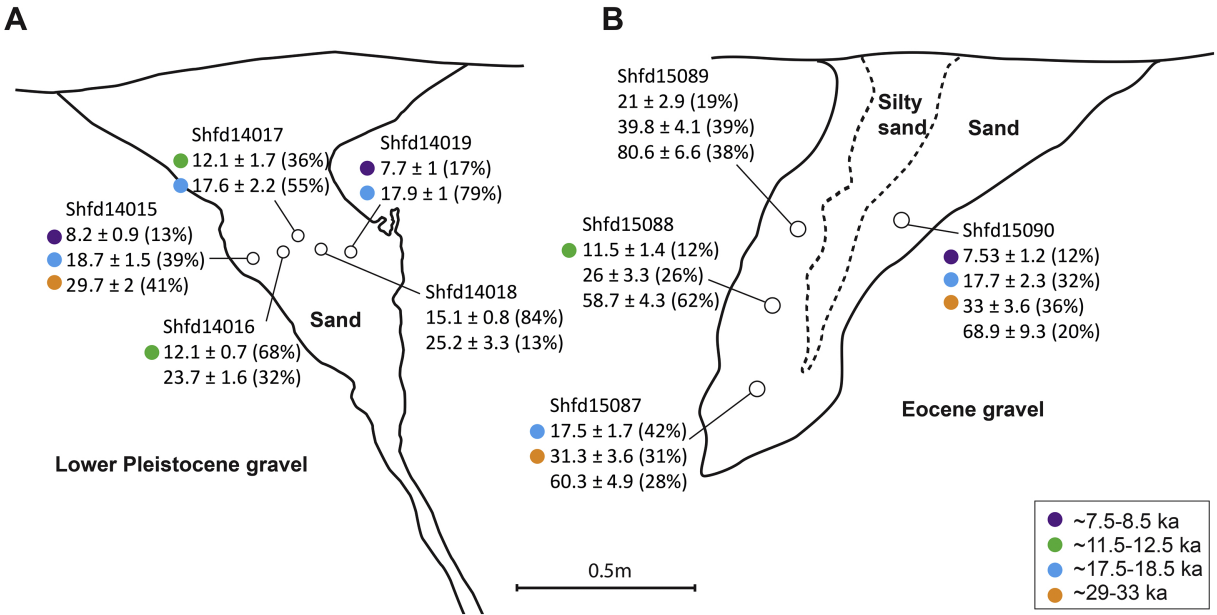
A
Shfd14017
12.1 ± 1.7 (36%)
17.6 ± 2.2 (55%)
Shfd14019
7.7 ± 1 (17%)
17.9 ± 1 (79%)
Shfd14015
8.2 ± 0.9 (13%)
18.7 ± 1.5 (39%)
29.7 ± 2 (41%)
Shfd14018
15.1 ± 0.8 (84%)
25.2 ± 3.3 (13%)
Shfd14016
12.1 ± 0.7 (68%)
23.7 ± 1.6 (32%)
Sand
Lower Pleistocene gravel
B
Shfd15089
21 ± 2.9 (19%)
39.8 ± 4.1 (39%)
80.6 ± 6.6 (38%)
Silty sand
Sand
Shfd15088
11.5 ± 1.4 (12%)
26 ± 3.3 (26%)
58.7 ± 4.3 (62%)
Shfd15090
7.53 ± 1.2 (12%)
17.7 ± 2.3 (32%)
33 ± 3.6 (36%)
68.9 ± 9.3 (20%)
Shfd15087
17.5 ± 1.7 (42%)
31.3 ± 3.6 (31%)
60.3 ± 4.9 (28%)
Eocene gravel
0.5m
~7.5-8.5 ka
~11.5-12.5 ka
~17.5-18.5 ka
~29-33 ka

Figure 6

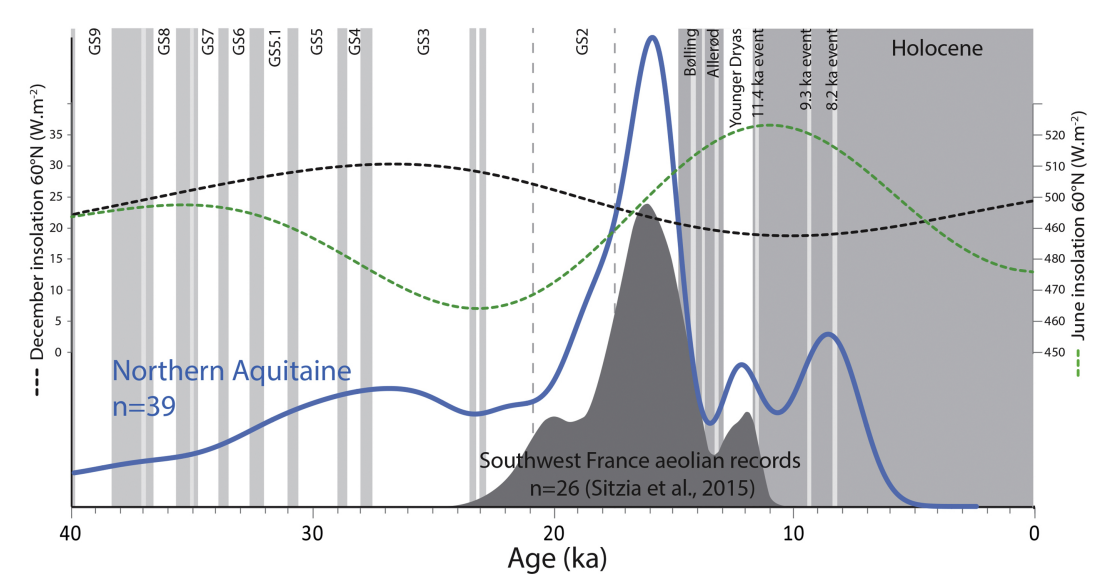
GS9
GS8
GS7
GS6
GS5.1
GS5
GS4
GS3
GS2
Bølling
Allerød
Younger Dryas
11.4 ka event
9.3 ka event
8.2 ka event
Holocene
December insolation 60°N (W.m-2)
June insolation 60°N (W.m-2)
Northern Aquitaine
n=39
Southwest France aeolian records
n=26 (Sitzia et al., 2015)
Age (ka)

Figure 7

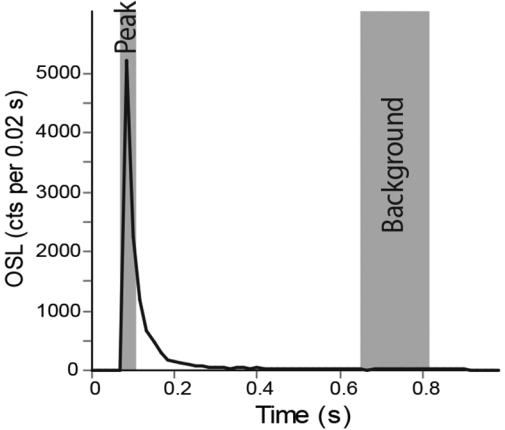
Peak
Background
OSL (cts per 0.02 s)
5000
4000
3000
2000
1000
0
0
0.2
0.4
0.6
0.8
Time (s)

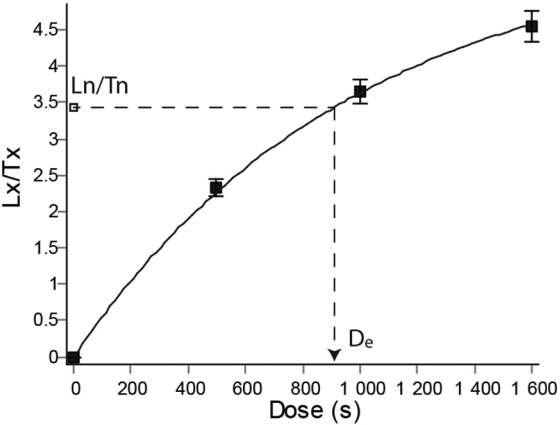
Ln/Tn
Lx/Tx
4.5
4
3.5
3
2.5
2
1.5
1
0.5
0
De
0
200
400
600
800
1 000
1 200
1 400
1 600
Dose (s)

Figure 8

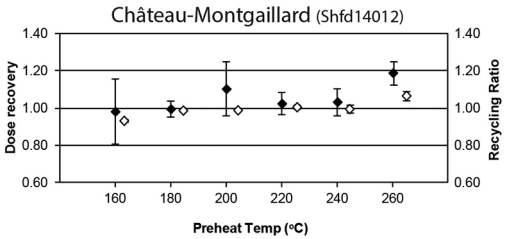
Château-Montgaillard (Shfd14012)
Dose recovery
Recycling Ratio
Preheat Temp (°C)

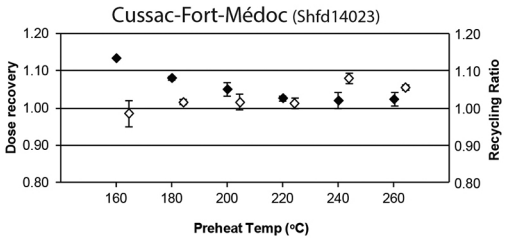
Cussac-Fort-Médoc (Shfd14023)
Dose recovery
Recycling Ratio
Preheat Temp (°C)

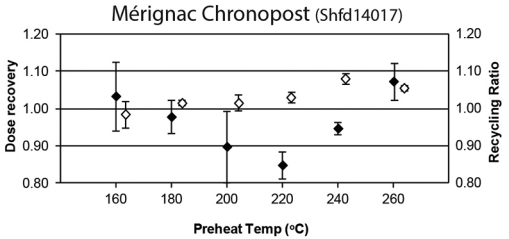
Mérignac Chronopost (Shfd14017)
Dose recovery
Recycling Ratio
Preheat Temp (°C)

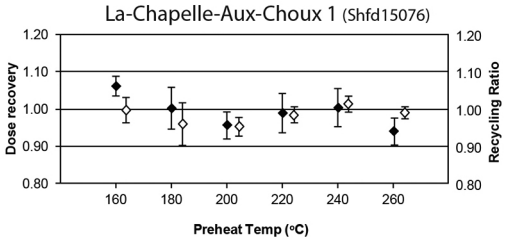
La-Chapelle-Aux-Choux 1 (Shfd15076)
Dose recovery
Recycling Ratio
Preheat Temp (°C)

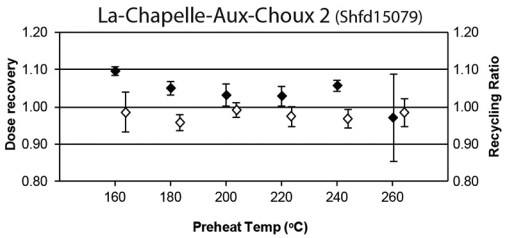
La-Chapelle-Aux-Choux 2 (Shfd15079)
Dose recovery
Recycling Ratio
Preheat Temp (°C)

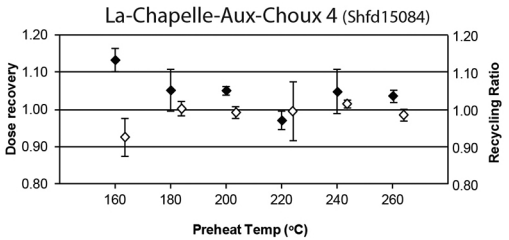
La-Chapelle-Aux-Choux 4 (Shfd15084)
Dose recovery
Recycling Ratio
Preheat Temp (°C)

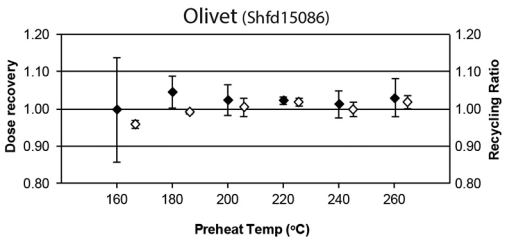
Olivet (Shfd15086)
Dose recovery
Recycling Ratio
Preheat Temp (°C)

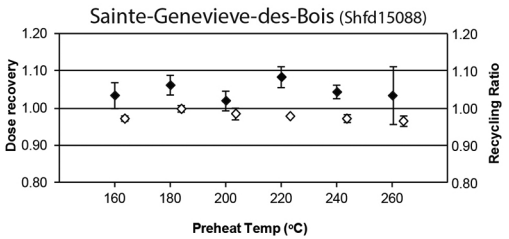
Sainte-Genevieve-des-Bois (Shfd15088)
Dose recovery
Recycling Ratio
Preheat Temp (°C)

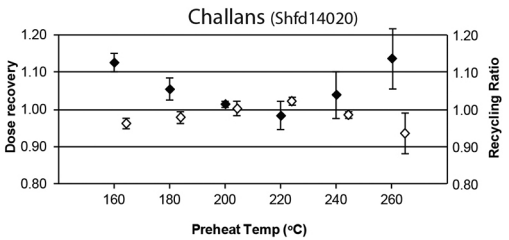
Challans (Shfd14020)
Dose recovery
Recycling Ratio
Preheat Temp (°C)

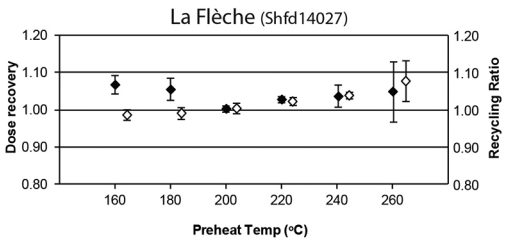
La Flèche (Shfd14027)
Dose recovery
Recycling Ratio
Preheat Temp (°C)

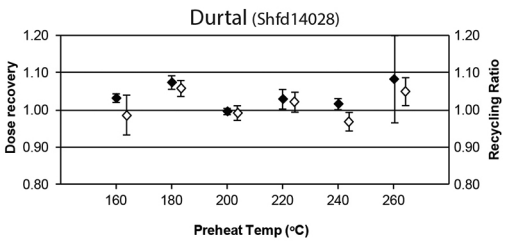
Durtal (Shfd14028)
Dose recovery
Recycling Ratio
Preheat Temp (°C)

Figure 9

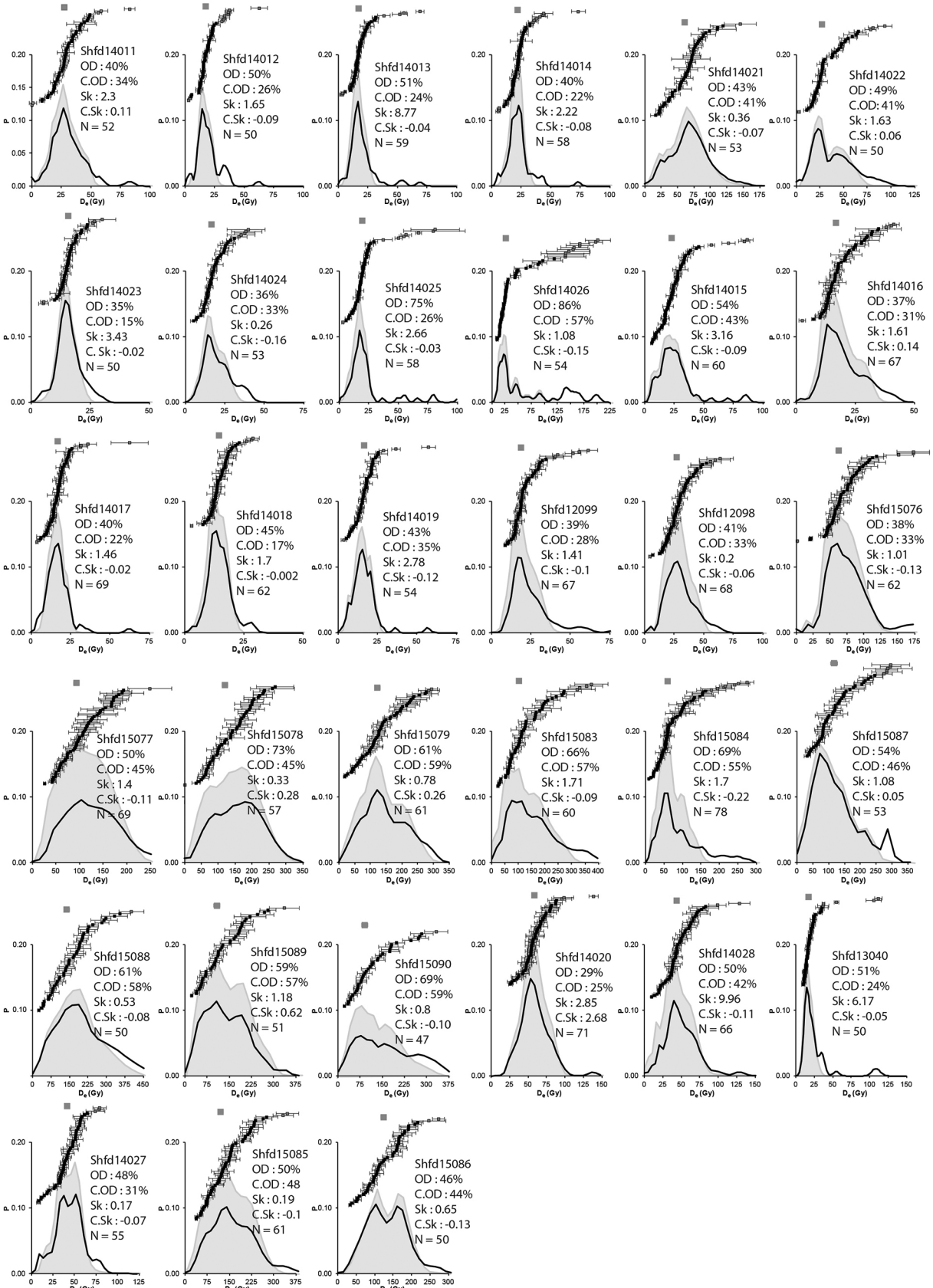
Shfd14011
OD : 40%
C.OD : 34%
Sk : 2.3
C.Sk : 0.11
N = 52
Shfd14012
OD : 50%
C.OD : 26%
Sk : 1.65
C.Sk : -0.09
N = 50
Shfd14013
OD : 51%
C.OD : 24%
Sk : 8.77
C.Sk : -0.04
N = 59
Shfd14014
OD : 40%
C.OD : 22%
Sk : 2.22
C.Sk : -0.08
N = 58
Shfd14021
OD : 43%
C.OD : 41%
Sk : 0.36
C.Sk : -0.07
N = 53
Shfd14022
OD : 49%
C.OD: 41%
Sk : 1.63
C.Sk : 0.06
N = 50
Shfd14023
OD : 35%
C.OD : 15%
Sk : 3.43
C. Sk : -0.02
N = 50
Shfd14024
OD : 36%
C.OD : 33%
Sk : 0.26
C.Sk : -0.16
N = 53
Shfd14025
OD : 75%
C.OD : 26%
Sk : 2.66
C.Sk : -0.03
N = 58
Shfd14026
OD : 86%
C.OD : 57%
Sk : 1.08
C.Sk : -0.15
N = 54
Shfd14015
OD : 54%
C.OD : 43%
Sk : 3.16
C.Sk : -0.09
N = 60
Shfd14016
OD : 37%
C.OD : 31%
Sk : 1.61
C.Sk : 0.14
N = 67
Shfd14017
OD : 40%
C.OD : 22%
Sk : 1.46
C.Sk : -0.02
N = 69
Shfd14018
OD : 45%
C.OD : 17%
Sk : 1.7
C.Sk : -0.002
N = 62
Shfd14019
OD : 43%
C.OD : 35%
Sk : 2.78
C.Sk : -0.12
N = 54
Shfd12099
OD : 39%
C.OD : 28%
Sk : 1.41
C.Sk : -0.1
N = 67
Shfd12098
OD : 41%
C.OD : 33%
Sk : 0.2
C.Sk : -0.06
N = 68
Shfd15076
OD : 38%
C.OD : 33%
Sk : 1.01
C.Sk : -0.13
N = 62
Shfd15077
OD : 50%
C.OD : 45%
Sk : 1.4
C.Sk : -0.11
N = 69
Shfd15078
OD : 73%
C.OD : 45%
Sk : 0.33
C.Sk : 0.28
N = 57
Shfd15079
OD : 61%
C.OD : 59%
Sk : 0.78
C.Sk : 0.26
N = 61
Shfd15083
OD : 66%
C.OD : 57%
Sk : 1.71
C.Sk : -0.09
N = 60
Shfd15084
OD : 69%
C.OD : 55%
Sk : 1.7
C.Sk : -0.22
N = 78
Shfd15087
OD : 54%
C.OD : 46%
Sk : 1.08
C.Sk : 0.05
N = 53
Shfd15088
OD : 61%
C.OD : 58%
Sk : 0.53
C.Sk : -0.08
N = 50
Shfd15089
OD : 59%
C.OD : 57%
Sk : 1.18
C.Sk : 0.62
N = 51
Shfd15090
OD : 69%
C.OD : 59%
Sk : 0.8
C.Sk : -0.10
N = 47
Shfd14020
OD : 29%
C.OD : 25%
Sk : 2.85
C.Sk : 2.68
N = 71
Shfd14028
OD : 50%
C.OD : 42%
Sk : 9.96
C.Sk : -0.11
N = 66
Shfd13040
OD : 51%
C.OD : 24%
Sk : 6.17
C.Sk : -0.05
N = 50
Shfd14027
OD : 48%
C.OD : 31%
Sk : 0.17
C.Sk : -0.07
N = 55
Shfd15085
OD : 50%
C.OD : 48
Sk : 0.19
C.Sk : -0.1
N = 61
Shfd15086
OD : 46%
C.OD : 44%
Sk : 0.65
C.Sk : -0.13
N = 50
P
De (Gy)

Figure 10

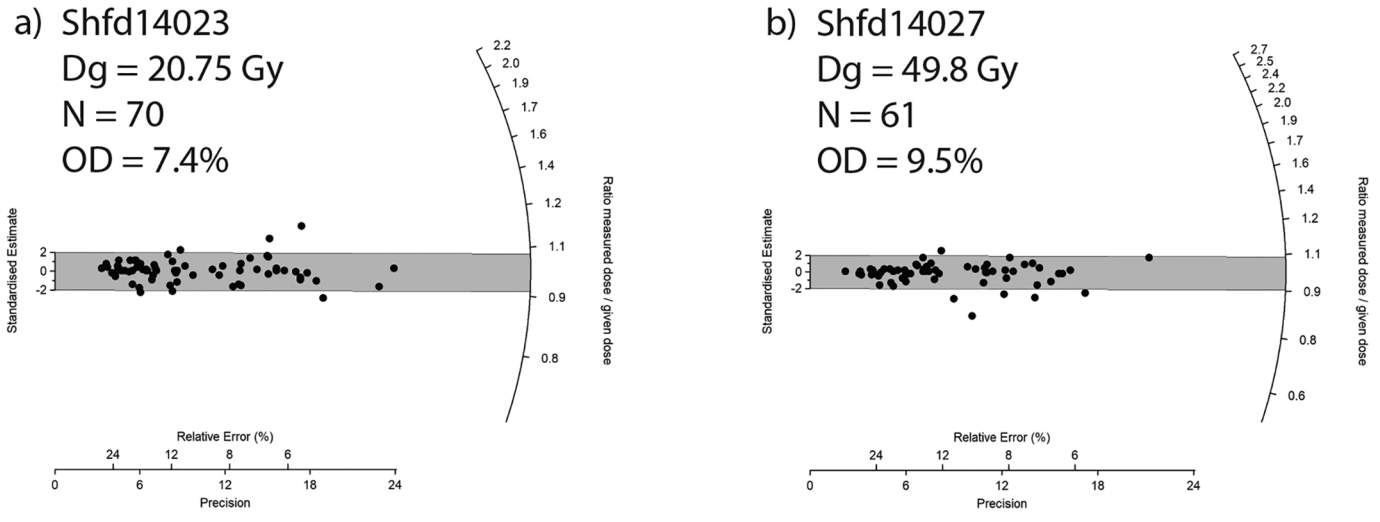
a) Shfd14023
Dg = 20.75 Gy
N = 70
OD = 7.4%
Standardised Estimate
2
0
-2
Ratio measured dose / given dose
2.2
2.0
1.9
1.7
1.6
1.4
1.2
1.1
0.9
0.8
Relative Error (%)
24
12
8
6
0
6
12
18
24
Precision
b) Shfd14027
Dg = 49.8 Gy
N = 61
OD = 9.5%
Standardised Estimate
2
0
-2
Ratio measured dose / given dose
2.7
2.5
2.4
2.2
2.0
1.9
1.7
1.6
1.4
1.2
1.1
0.9
0.8
0.6
Relative Error (%)
24
12
8
6
0
6
12
18
24
Precision

Figure 11